Chaos, 55–95

Poincaré Seminar 2010

Chaotic Dynamos Generated by Fully Turbulent Flows

Stéphan Fauve

Abstract. We report experimental results on the generation of a magnetic field by the motion of an electrically conducting liquid metal. We recall that this dynamo effect is a canonical example of an instability process that occurs on a strongly turbulent flow. Although the magnetic field is driven by a turbulent velocity field that involves a wide range of interacting scales, we observe that its dynamics results from a small number of interacting modes. We present a model that describes both periodic and random reversals of the magnetic field and compare it with the experimental results and direct numerical simulations.

1. Introduction

Until the seventies, it was believed that an erratic temporal behavior of some quantity $x(t)$ in a statistically stationary state had to result from the interaction of many degrees of freedom. For instance, a qualitative description of the transition to turbulence of fluid flows given by Landau & Lifshitz (1959) was ascribing the temporal complexity to the arbitrary phases resulting from a large number of successive Hopf bifurcations. Most quantitative models of systems with an erratic behavior were based on the theory of stochastic processes, assuming more or less explicitly that their randomness was resulting from a large number of uncontrolled parameters or initial conditions. It was of course known since Poincaré that low-dimensional Hamiltonian systems can display complicated (non periodic) solutions, iterations of simple maps were used to generate random numbers, and erratic behaviors were observed in simple electric devices, but the concept of low-dimensional deterministic chaos was far from being considered among physicists who were used to problems either governed by linear equations, or constrained by extremum principles. Modeling an erratic temporal behavior with a low-dimensional dynamical system, i.e., a small number of coupled nonlinear differential equations, has been made first in the sixties, one of the most famous example being the Lorenz system

(Lorenz 1963), which certainly triggered a large part of the studies on temporal chaos that were performed in the seventies and the eighties. Ruelle and Takens (1971) proposed a qualitative mechanism to get a chaotic regime after a small number of bifurcations from a stationary state, in contrast to Landau's picture. A chaotic velocity field in a Couette–Taylor flow, generated from a stationary state after a small number of transitions, was reported by Swinney & Gollub (1975) and followed by a lot of similar observations in other hydrodynamic systems, nonlinear electronic, acoustic or optical devices, chemical reactions, etc. The observation of the period doubling transition scenario to chaos in a flow driven by thermal convection by Maurer and Libchaber (1979) opened the way to test quantitative predictions made using renormalisation group techniques on the logistic map (Feigenbaum 1978, Tresser & Coullet 1978). The observed quantitative agreement (Libchaber *et al.* 1982) clearly showed that the flow of a viscous fluid can display a transition to an erratic temporal behavior that is qualitatively and quantitatively described by a small number of interacting modes or degrees of freedom. Other transition scenarios to chaos were predicted, such as intermittency (Manneville & Pomeau 1979) or transitions from quasiperiodic states that were also found in good quantitative agreement with experimental observations in many different systems. The general picture that emerged from these experimental and theoretical studies is that there exist universal scenarios of transition to chaos. Similarly to phase transitions, there are quantitative characteristics of these scenarios that do not depend on the particular system under consideration.

However, in contrast to what has been believed for a while by some people, these achievements did not help to solve the problem of fluid turbulence. It has been realized that one usually needs to quench a lot of degrees of freedom of a fluid flow in order to observe chaotic regimes in agreement with the behaviors predicted for low-dimensional dynamical systems. For instance, the convection experiments mentioned above were performed in containers of small aspect ratio, i.e., involving a small number of convective rolls. In the case of large aspect ratio containers, no simple scenario of transition to chaos was identified (Ahlers & Behringer 1978). A more flexible way to control the number of degrees of freedom of a convective flow has been used by applying an external horizontal magnetic field to an electrically conducting fluid. This inhibits three-dimensional modes and makes the flow two-dimensional without variation of the velocity along the magnetic field axis. It has been shown that transitions to chaos in agreement with the behaviors predicted by low-dimensional dynamical systems were observed only for large enough values of the applied magnetic field (Fauve *et al.* 1984). Thus, although dynamical system theory provided new concepts in physics including the one of deterministic chaos, and triggered a new way of approaching nonlinear phenomena, it has been so far of little help to understand turbulent flows which involve the interaction of many different scales. Kolmogorov type qualitative arguments or a stochastic description are more efficient tools in these cases. This has given the impression that despite its success, deterministic chaos is restricted to a class of rather academic flows in which many degrees of freedom have been quenched.

On the other hand, it can be argued that the dynamics of some large scale modes in a strongly turbulent flow could display low-dimensional dynamics if they are weakly coupled to the turbulent background. This is the case in many geophysical and astrophysical flows where an oscillatory or a weakly chaotic behavior can occur in flows at huge Reynolds numbers. Some climatic phenomena indeed display a characteristic feature of low-dimensional chaos: well defined patterns occur within a random temporal behavior. Examples are atmospheric blockings that can affect the climate on a time scale of several days (Ghil & Childress 1987) or El Nino events that occur every few years (Vallis 1986). The qualitative features of these phenomena have been often modeled using a few coupled variables such as mean temperature, wind or current. This truncation is sometimes justified by scale separation (for instance, the dynamics of the ocean is much slower than the one of the atmosphere), but it is often arbitrary since many phenomena involve a continuum of scales without any clear gap among them. Another example of nearly periodic behavior superimposed on turbulence is provided by the solar cycle: it has been observed since several centuries that well-defined spatio-temporal patterns, dark spots on the solar surface that appear at mid-latitudes and migrate toward the equator, involve a 22 year period. It has been found later that these spots correspond to large values of the magnetic field generated by turbulent convection in the sun through the dynamo effect. The number of sun spots follows the cycle of the solar magnetic field that reverses roughly every 11 years. The amplitude of this oscillation varies on much longer time scales, and long periods with a very low solar activity (a small number of sun spots) randomly occurred in the past. Several low-dimensional models of the solar cycle, involving a few modes of the magnetic and velocity fields, have been proposed (see Section 5). It is very hard to justify this type of description; the level of turbulence is so high that both the velocity and the magnetic fields display a continuous range of scales and it looks rather arbitrary to write down a few equations for a small number of modes and forget about the effect of all the others.

It is known that the dynamics of a complex system is governed by a small number of relevant modes in the vicinity of bifurcations (see for instance, Arnold 1982). The amplitude of the unstable modes varying on long time scales compared to the stable ones, the later can be adiabatically eliminated, thus leading to a low-dimensional dynamical system. There exist various perturbation techniques that can be used to perform this elimination and find the differential equations governing the amplitudes of the unstable modes when the basic state of the system is stationary or time periodic. However, almost nothing is known when an instability occurs from a turbulent regime. It seems even difficult to give a proper definition of such a situation in hydrodynamic turbulence. The dynamo effect, i.e., the generation of a magnetic field by the flow of an electrically conducting fluid, provides a very interesting situation in this respect. It is an instability process that can occur in a liquid metal only when the kinetic Reynolds number of the flow is very large (see Section 2). The instability threshold can be easily defined. Although the experiments involve some cost and technical difficulties, once the dynamo regime is

reached, the dynamics of the magnetic field can be easily measured. We will show here that even when the magnetic field is generated by a strongly turbulent flow that involves fluctuations as large as the mean flow, it displays low-dimensional dynamics. Thus, fluid dynamos provide an example in which a few modes are governed by a low-dimensional dynamical system although they are coupled to a strongly turbulent background.

This paper is organized as follows: definitions and elementary facts about fluid dynamos are shortly recalled in Section 2. In Section 3, the first experimental observations made in Karlsruhe and Riga are described. The results of the VKS experiment are reported in Section 4. Section 5 provides a short review of the phenomenon of magnetic reversals and of various related models. A model for the dynamics of the magnetic field observed in the VKS experiment is presented is Section 6. It is illustrated using direct numerical simulations in Section 7. Finally, a minimal model for field reversals is presented in Section 8. Some other systems displaying a low-dimensional large scale dynamics on a turbulent background are mentioned in the conclusion.

2. The dynamo effect

It is now believed that magnetic fields of planets and stars are generated by the motion of electrically conducting fluids through the dynamo process. This has been first proposed by Larmor (Larmor, 1919) for the magnetic field of the sun. Assuming the existence of an initial perturbation of magnetic field, he observed that "internal motion induces an electric field acting on the moving matter: and if any conducting path around the solar axis happens to be open, an electric current will flow round it, which may in turn increase the inducing magnetic field. In this way it is possible for the internal cyclic motion to act after the manner of the cycle of a self-exciting dynamo, and maintain a permanent magnetic field from insignificant beginnings, at the expense of some of the energy of the internal circulation" (for reviews of the subject, see for instance Moffatt (1978), Zeldovich *et al.* (1983), Busse (1977), Roberts (1994), Fauve & Pétrélis (2003).

Maxwell's equations together with Ohm's law give the governing equation of the magnetic field, $\mathbf{B}(\mathbf{r},t)$. In the approximation of magnetohydrodynamics (MHD), it takes the form

$$\frac{\partial \mathbf{B}}{\partial t} = \nabla \times (\mathbf{V} \times \mathbf{B}) + \frac{1}{\mu_0 \sigma} \nabla^{\mathbf{2}} \mathbf{B}, \tag{1}$$

where μ_0 is the magnetic permeability of vacuum and σ is the electrical conductivity. The last term on the right hand side of (1) represents ohmic dissipation, and the first one, electromagnetic induction due to the velocity field $\mathbf{V}(\mathbf{r},t)$. $B = 0$ is an obvious solution of (1), and for $V = 0$, any perturbation of $\mathbf{B}(\mathbf{r},t)$ (respectively of the current density $\mathbf{j}(\mathbf{r},t)$) decays to zero due to ohmic diffusion. $B = 0$ can be an unstable solution if the induction term compensates ohmic dissipation. The ratio of these two terms defines the magnetic Reynolds number, $R_m = \mu_0 \sigma V L$,

where V is the typical velocity amplitude and L the typical length scale of the flow. If $\mathbf{V}(\mathbf{r},t)$ has an appropriate geometry, perturbations of magnetic field grow when R_m becomes larger than a critical value R_m^c (in the range 10–1000 for most studied examples). Magnetic energy is generated from part of the mechanical work used to drive the flow.

In order to describe the saturation of the magnetic field above the dynamo threshold R_m^c, we need to take into account its back reaction on the velocity field. $\mathbf{V}(\mathbf{r},t)$ is governed by the Navier–Stokes equation

$$\frac{\partial \mathbf{V}}{\partial t} + (\mathbf{V}\cdot\nabla)\mathbf{V} = -\nabla\left(\frac{p}{\rho} + \frac{B^2}{2\mu_0\rho}\right) + \nu\nabla^2\mathbf{V} + \frac{1}{\mu_0\rho}(\mathbf{B}\cdot\nabla)\mathbf{B}, \tag{2}$$

that we have restricted to the case of an incompressible flow ($\nabla\cdot\mathbf{V}=0$). ν is the kinematic viscosity and ρ is the fluid density. In the MHD approximation, the Lorentz force, $\mathbf{j}\times\mathbf{B}$, can be split into the two terms involving $\mathbf{B}$ in (2). If the modification of the flow under the action of the growing magnetic field weakens the dynamo capability of the flow, the dynamo bifurcation is supercritical, i.e., the magnetic field grows continuously from zero when R_m is increased above R_m^c.

Thus, the minimum set of parameters involved in a fluid dynamo consists of the size of the flow domain, L, the typical fluid velocity, V, the density, ρ, the kinematic viscosity, ν, the magnetic permeability of vacuum, μ_0, and the fluid electrical conductivity, σ. For most astrophysical objects, the global rotation rate, Ω, also plays an important role and the Coriolis force $-2\boldsymbol{\Omega}\times\mathbf{V}$ should be taken into account when the Navier–Stokes equation (2) is written in the rotating frame. Three independent dimensionless parameters thus govern the problem. We can choose the magnetic Reynolds number, R_m, the magnetic Prandtl number, P_m, and the Rossby number Ro

$$R_m = \mu_0\sigma V L, \quad P_m = \mu_0\sigma\nu, \quad Ro = \frac{V}{L\Omega}. \tag{3}$$

Then, dimensional analysis implies that we have for the dynamo threshold

$$R_m^c = f(P_m, Ro), \tag{4}$$

and for the mean magnetic energy generated above the dynamo threshold

$$\langle B^2\rangle = \mu_0\rho V^2\, g(R_m, P_m, Ro). \tag{5}$$

f and g are arbitrary functions at this stage. Their dependence on P_m (or equivalently on the kinetic Reynolds number, $Re = VL/\nu$) and on Ro can be related to the effect of flow characteristics (in particular turbulence) on the dynamo threshold and saturation. In many realistic situations, more parameters should be taken into account. For instance, f and g also depend on the choice of boundary conditions (for instance their electrical conductivity or their magnetic permeability, etc).

For planets and stars as well as for all liquid metals in the laboratory, the magnetic Prandtl number is very small, $P_m < 10^{-5}$. Magnetic field self-generation can be obtained only for large enough values of R_m for which Joule dissipation can

be overcome (for most known fluid dynamos, the dynamo threshold R_{mc} is roughly in the range 10–1000). Therefore, the kinetic Reynolds number, $Re = R_m/P_m$, is very large and the flow is strongly turbulent. This is of course the case of planets and stars which involve huge values of Re but is also true for dynamo experiments with liquid metals for which $Re > 10^5$. Direct numerical simulations are only possible for values of P_m orders of magnitude larger that the realistic ones for the sun, the Earth or laboratory experiments. First because it is not possible to handle a too large difference between the time scale of diffusion of the magnetic field and the one of momentum; second, a small P_m dynamo occurs for large Re and requires the resolution of the small spatial scales generated by turbulence. Strongly developed turbulence has also some cost for the experimentalists. Indeed, the power needed to drive a turbulent flow scales like $P \propto \rho L^2 V^3$ and we have

$$R_m \propto \mu_0 \sigma \left(\frac{PL}{\rho} \right)^{1/3}. \tag{6}$$

This formula has simple consequences: first, taking liquid sodium (the liquid metal with the highest electric conductivity), $\mu_0 \sigma \approx 10\ m^{-2} s$, $\rho \approx 10^3\, kg\, m^{-3}$, and with a typical length-scale $L \approx 1$m, we get $P \approx R_m^3$; thus a mechanical power larger than 100 kW is needed to reach a dynamo threshold of the order of 50. Second, it appears unlikely to ever operate experimental dynamos at R_m large compared with R_{mc}. Indeed, it costs 8 times more power to reach $2R_{mc}$ than to reach the dynamo threshold. In conclusion, most experimental dynamos should have the following characteristics:

- they bifurcate from a strongly turbulent flow regime,
- they operate in the vicinity of their bifurcation threshold.

Although the values of R_m and P_m that can be obtained in laboratory experiments using liquid sodium are not too far from the ones of the Earth core, it would be very difficult to perform experiments with large R_m at Ro significantly smaller than unity whereas we have $Ro \approx 10^{-6}$ for the Earth core. The comparison is of course also difficult in the case of the sun: although Ro is of order one for the solar convection zone, R_m is more than six orders of magnitude larger than in any laboratory experiment. As said above, the situation is worse when direct numerical simulations are considered. We thus cannot claim that cosmic magnetic fields can be reproduced at the laboratory scale except if we can show that the dynamics of the magnetic field weakly depends on some dimensionless parameters.

As already mentioned, laboratory dynamos operate in the vicinity of the instability threshold but at very high values of the Reynolds number. This give rise to a very interesting example of instability that differs in many respects from usual hydrodynamical instabilities. The dynamo bifurcation occurs from a base state which is fully turbulent. This may play a role on various aspects of the dynamo process and it raises several questions.

- What is the effect of turbulent velocity fluctuations on the dynamo onset? Can they change the nature of the bifurcation? Will they favor or inhibit

dynamo action? In other words, what is the behavior of f when $P_m \to 0$? In the absence of global rotation, $Ro^{-1} = 0$, is f constant with respect to P_m in this limit, thus giving R_m^c = constant, or does the threshold continuously increases when $P_m \to 0$? (Fauve & Pétrélis, 2007).

- Above onset, at which amplitude does the magnetic field saturate? In the absence of global rotation and for small P_m, do we have $\langle B^2 \rangle \propto \mu_0 \rho V^2 g(R_m)$, i.e., $\langle B^2 \rangle \propto [\rho/(\mu_0 \sigma^2 L^2)]\, g(R_m)$ close to threshold (Pétrélis & Fauve 2001)?
- Is there a parameter range for which we get energy equipartition, $\langle B^2 \rangle / \mu_0 \propto \rho V^2$? What is the behavior of the ohmic to viscous dissipation ratio? (Fauve & Pétrélis 2007).
- What is the effect of global rotation on the dynamo threshold and saturation?
- What is the effect of turbulent fluctuations on the bifurcation? Is $g(R_m) \propto R_m - R_m^c$ as for a usual supercritical bifurcation close to threshold, or should we expect a behaviour involving an anomalous exponent (Pétrélis *et al.* 2007)?
- What is the effect of turbulent fluctuations on the dynamics of the magnetic field? What are the statistical properties of the fluctuations of the magnetic field?

We will discuss these problems in connection with existing laboratory dynamo experiments. The first ones, performed in Karlsruhe and Riga, have been designed by taking into account the mean flow alone. Large scale turbulent fluctuations have been inhibited as much as possible by a proper choice of boundary conditions. On the contrary, the VKS experiment has been first motivated by the study of the possible effects of turbulence on the dynamo instability.

3. The Karlsruhe and Riga experiments

The first homogeneous fluid dynamos have been operated in liquid sodium in Karlsruhe (Stieglitz and Müller, 2001) using a flow in an array of pipes set-up in order to mimic a spatially periodic flow proposed by G.O. Roberts (1972), and in Riga (Gailitis *et al.*, 2001) using a Ponomarenko-type flow (Ponomarenko, 1973). We first recall the flow geometries and briefly review the results obtained by both groups.

3.1. The Karlsruhe experiment

The experiment in Karlsruhe, Germany, was motivated by a kinematic dynamo model developed by G.O. Roberts (Roberts, 1972) who showed that various periodic flows can generate a magnetic field at large scale compared to the flow spatial periodicity. One of the cellular flows he considered is a periodic array of vortices with the same helicity. Flows with such topology drive an α-effect that can lead to dynamo action. This mechanism is quite efficient at self-generation (in the sense of generating a magnetic field at a low magnetic Reynolds number based on the wavelength of the flow).

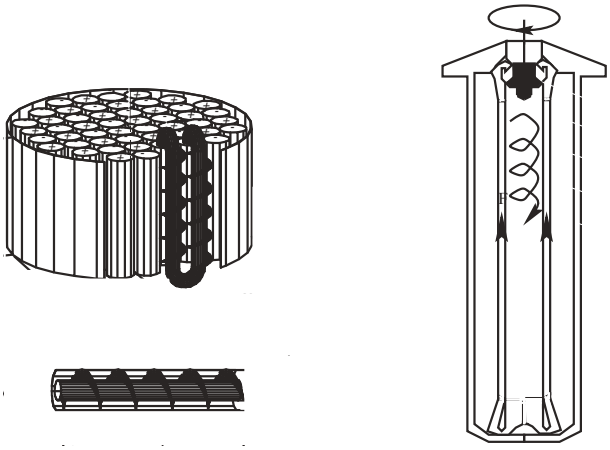

(a) (b)

FIGURE 1. Schematics for the experiments from Karlsruhe (a) and Riga (b) which show how helical flow is forced by guiding the sodium through steel channels. From [88] with permission from © 2001 The American Physical Society.

A dynamo based on this mechanism was constructed and run successfully in Karlsruhe. A sketch of the experiment is shown in Figure 1a. The flow is located in a cylindrical vessel of width 1.85 m and height $H = 0.7$ m. It contains 52 elementary cells placed on a square lattice. Each cell is made of two coaxial pipes: an helical baffle drives the helical flow in the outer cylindrical shell whereas the flow in the inner shell is axial. In two neighbouring cells, the velocities are opposite such that the helicity has the same sign in all the cells. Although the volume is finite instead of the infinite extension assumed by G.O. Roberts, the dynamo capability of the flow is not strongly affected in the limit of scale separation, i.e., when the size L of the full volume is large compared to the wavelength l of the flow (Busse *et al.*, 1996). In this limit, the relevant magnetic Reynolds number involves the geometrical mean of the two scales as a length-scale, and the geometrical mean of axial and azimuthal velocities as a velocity scale. However, it can be shown using simple arguments that it is not efficient to increase too much the scale separation if one wants to minimise the power needed to reach the dynamo threshold (Fauve and Pétrélis, 2003). The flow is driven by three electromagnetic pumps and the axial and azimuthal velocities are independently controlled. The liquid sodium temperature is maintained fixed by three steam-evaporation heat exchangers. Measurements of the magnetic field were made both locally with Hall-probes and globally using wire coils. Pressure drops in the pipe and local velocity measurements were also performed.

When the flow rates are large enough, a magnetic field is generated by dynamo action. The bifurcation is stationary and the magnetic field displays fluctuations

caused by the small scale turbulent velocity field (see Figure 2). This generation comes at a cost in the power necessary to drive the flow and the pressure drop increases.

Due to the Earth's magnetic field, the bifurcation is imperfect but both branches of the bifurcation can be reached by applying an external magnetic field, as displayed in Figure 2. Among others, the experimentalists performed careful studies of the dependence of the dynamo threshold on the axial and helical flow rates and on the electrical conductivity that can be varied by changing the temperature. They also considered the effect of flow modulation on the dynamo threshold and studied the amplitude and the geometry of the magnetic field in the supercritical regime.

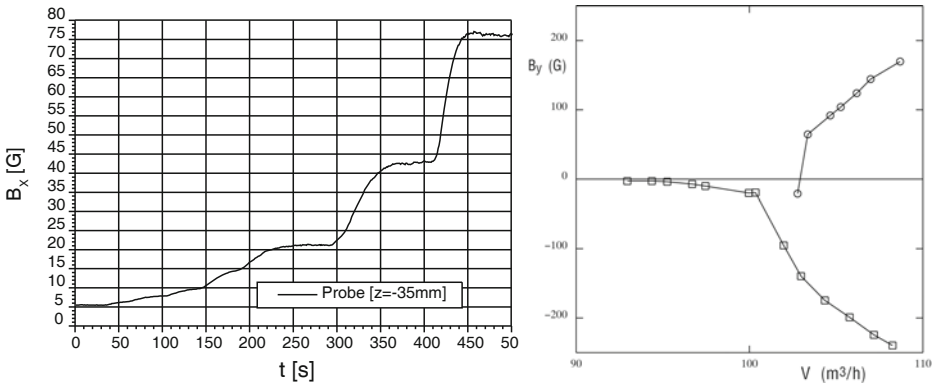

FIGURE 2. (Left) Time recording of one component of the magnetic field in the Karlsruhe experiment. The amplitude of the magnetic field increases after each increasing step of the flow rate of liquid sodium. Small fluctuations are visible once the magnetic field has saturated at a constant mean value. (Right) The magnetic field amplitude increases above the critical flow rate. Another branch of self-generation can be reached only by imposing an initial field. This other branch is disconnected from the main branch. The imperfection of the bifurcation has been ascribed to the Earth's field. From [89] with permission from © 2002 Institute of Physics, University of Latvia.

3.2. The Riga experiment

The experiment carried out by Gailitis *et al.* (2001) has been motivated by one of the simplest examples of a homogeneous dynamo found by Ponomarenko (1973). A conducting cylinder of radius R, embedded in an infinite static medium of the same conductivity with which it is in perfect electrical contact, is in solid body rotation at angular velocity Ω, and in translation along its axis at speed V. In an unbounded domain, this helical motion generates a travelling wave

magnetic field. This Hopf bifurcation occurs for a minimum critical magnetic Reynolds number $R_{mc} = \mu_0 \sigma R \sqrt{(R\omega)^2 + V^2} = 17.7$ for an optimum Rossby number $Ro = V/(R\Omega) = 1.3$. We note that the maximum dynamo capability of the flow (R_{mc} minimum) is obtained when the azimuthal and axial velocities are of the same order of magnitude ($Ro \sim 1$). This trend is often observed with more complex flows for which the maximum dynamo capability is obtained when the poloidal and toroidal flow components are comparable.

The experiment set up by the Riga group is sketched in Figure 1b. Their flow is driven by a single propellor, generating helical flow down a central cylindrical cavity. The return flow is in an annulus surrounding this central flow. The geometry of the apparatus as well as mean flow velocity profiles have been optimized in order to decrease the dynamo threshold. In particular, it has been found that adding an outer cylindrical region with liquid sodium at rest significantly decreases R_{mc}. This can be understood if the axial mean flow as well as the rotation rate of the azimuthal mean flow are nearly constant except in boundary layers close to the inner cylinder. Then, the induction equation being invariant under transformation to a rotating reference frame and under Galilean transformations, the presence of some electrical conductor at rest is essential as it is in the case of the Ponomarenko dynamo. The three cylindrical chambers are separated by thin stainless steel walls, which were wetted to allow currents to flow through them.

Figure 3 displays the growth and saturation of a time periodic magnetic field at high enough rotation rate. The nature of the bifurcation as well as dynamo growth rates have been found in good agreement with kinematic theory (Gailitis *et al.*, 2002) that predicts a Hopf bifurcation of convective nature at onset. In addition, the Riga group has made detailed observations of the magnetic field saturation value and the power dissipation needed to drive the flow. These measurements give indications of the effect of Lorentz forces in the flow in order to reach the saturated state. It has been found that one effect of the Lorentz force is to drive the liquid sodium in the outer cylinder in global rotation, thus decreasing the effective azimuthal velocity of the inner flow and therefore its dynamo capability. Dynamo generation does also correspond to an increase in the required mechanical power. However, a puzzling result is displayed in Figure 3: the amplitude of the magnetic field for supercritical rotation rates does not seem to show the universal $\sqrt{R_m - R_{mc}}$ law. In addition, the form of the law seems to depend on the location of the measurement point. This is to some extent due to the absence of temperature control in the Riga experiment. Variations in temperature modify the fluid parameters (electrical conductivity, viscosity and density) and this should be taken into account by plotting the results in dimensionless form (Fauve & Lathrop, 2005).

3.3. What have been learnt from the Karlsruhe and Riga experiments

Although there were no doubts about self-generation of magnetic fields by Roberts' or Ponomarenko-type laminar flows, these experiments have displayed several interesting features:

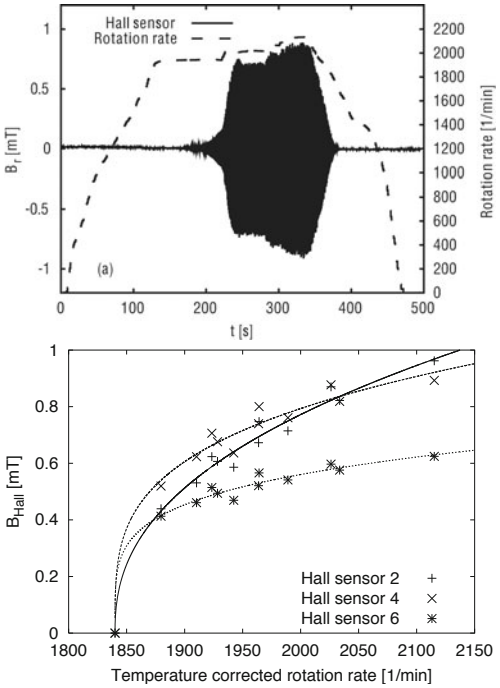

FIGURE 3. (Top) Time recording of the magnetic field from the Riga experiment. The dashed line gives the value of the rotation rate. The amplitude of roughly sinusoidal oscillations (not visible with the resolution of the picture) increases and then saturates when the rotation rate is increased above threshold (about 1850 rpm). The amplitude of saturation increases when the rotation rate is increased further. The dynamo switches off when the rotation rate is decreased below threshold. (Bottom) Magnetic field amplitude as the rotation rate is raised above the critical rotation rate. From [88] with permission from © 2001 The American Physical Society.

- the observed thresholds are in rather good agreement with theoretical predictions (Busse *et al.* 1996, Rädler *et al.*, 1998, Gailitis *et al.*, 2002) made by considering only the laminar mean flow and neglecting the small-scale turbulent fluctuations that are present in both experiments.
- The nature of the dynamo bifurcation, stationary for the Karlsruhe experiment or oscillatory (Hopf) in the Riga experiment, is also in agreement with laminar models.
- On the contrary, the saturation level of the magnetic field, due to the back reaction of the Lorentz force on the flow, cannot be predicted with a laminar flow model and different scaling laws exist in the supercritical dynamo regime

depending on the magnitude of the Reynolds number (Pétrélis and Fauve, 2001).
- Although secondary instabilities generating large scale dynamics of the magnetic field have not been observed in the Karlsruhe and Riga experiments, small scale turbulent fluctuations of the magnetic field are well developed.

These observations raise the following questions:

- What is the effect of turbulence, or of the magnitude of the Reynolds number, on the dynamo threshold R_{mc}? Is it possible to observe how R_{mc} depends on P_m for a dynamo generated by a strongly turbulent flow (by changing P_m in experiments with a given flow at different temperatures for instance)?
- What is the mechanism responsible for magnetic field fluctuations in the vicinity of the dynamo threshold: an on-off intermittency effect (Sweet *et al.*, 2001) or the advection of the mean magnetic field by the turbulent flow?
- What is the mechanism for field reversals? Is it possible to observe them in laboratory experiments?

4. The VKS experiment

4.1. A bifurcation from a strongly turbulent flow

Using the Reynolds decomposition, we can write for a turbulent velocity field

$$\mathbf{V}(\mathbf{r},\mathbf{t}) = \overline{\mathbf{V}}(\mathbf{r}) + \tilde{\mathbf{v}}(\mathbf{r},\mathbf{t}), \tag{7}$$

where $\overline{\mathbf{V}}(\mathbf{r})$ is the mean flow and $\tilde{\mathbf{v}}(\mathbf{r},\mathbf{t})$ are the turbulent fluctuations. The overbar stands for a temporal average in experiments. Thus, both the mean flow $\overline{\mathbf{V}}(\mathbf{r})$ and the fluctuations $\tilde{\mathbf{v}}(\mathbf{r},\mathbf{t})$ are involved in the induction term of (1) and one has to understand their respective effects on the dynamo process. The Karlsruhe and Riga experiments have been designed by geometrically constraining a mean flow $\overline{\mathbf{V}}(\mathbf{r})$ known for its efficient dynamo action, the G.O. Roberts' flow (respectively the Ponomarenko flow) for the Karlsruhe (respectively Riga) experiment. Turbulent fluctuations, roughly an order of magnitude smaller than the mean flow, have been discarded, and the experimentally observed dynamo threshold as well as the geometry of the mean magnetic field, have been found in good agreement with these predictions, based only the mean flow.

As explained in the introduction, one of my early motivations for dynamo experiments have been the study of a system that displays a bifurcation from a strongly turbulent regime. Thus, I chose to try to generate a dynamo using a von Karman swirling flow, i.e., the flow generated in a cylinder by the motion of two coaxial rotating discs (Zandbergen & Dijkstra 1987). When the discs are operated in counter-rotation, these flows display various qualities of interest for a potential dynamo: a strong differential rotation and the lack of planar symmetry which are key ingredients for a closed loop induction by ω and α effects (Moffatt 1978). As shown by measurements of pressure fluctuations, large vorticity concentrations are produced (Fauve *et al.* 1993, Abry *et al.* 1994) which may also act in favour of

the amplification of the magnetic field if the classical analogy between vorticity and magnetic field production is to be believed. The choice of VK flows was thus motivated by the hope that the above features will make possible the generation a magnetic field by a strongly turbulent flow, with fluctuations as large, or even larger than the mean flow.

4.2. The VKS experimental set-up

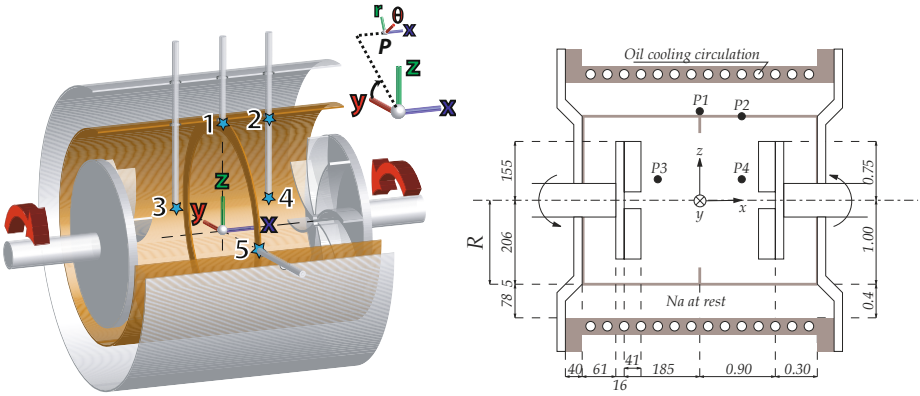

FIGURE 4. Experimental setup. From [58] with permission from © 2009 AIP Publishing LLC.

The VKS acronym stands for "von Kármán Sodium". The experiments has been developed in a collaborative work involving several french institutions: Direction des Sciences de la Matière of CEA, ENS-Lyon and ENS-Paris and have been realized in CEA/Cadarache-DEN/DTN. The VKS2 experiment is an evolution of a first design, VKS1 (Bourgoin *et al.* 2002, Pétrélis *et al.* 2003) which did not show any dynamo action. A sketch of the VKS2 set-up is displayed in Figure 4. The VK flow is generated in the inner cylinder of radius 206 mm and length 524 mm by two counter rotating discs of radius 154 mm and 371 mm apart. The disks are made of soft iron and are fitted with 8 curved blades of height $h = 41.2$ mm. An annulus of inner diameter 175 mm and thickness 5 mm is attached along the inner cylinder in the mid-plane between the disks.

This last configuration enabled the observation of a dynamo field as shown in Figure 5 (Monchaux *et al.* 2007). As the rotation rate of the discs is increased from 10 to 22 Hz, one observes at the location (1) (see Figure 4) the growth of a magnetic field: the azimuthal component acquires a nonzero average value of order 40 Gauss with relatively strong fluctuations. The two other components display small average values but fluctuate with *rms* values of order 5 gauss. Even though the fluctuation level is much higher than in the Karlsruhe or Riga experiments, we call this dynamo stationary in the sense that it is not displaying any kind of time-periodicity or reversals.

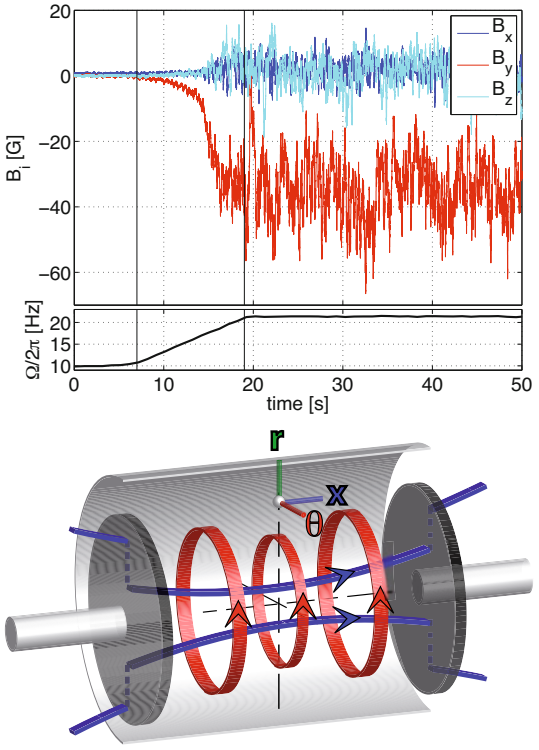

FIGURE 5. Three components of the magnetic field generated by dynamo action measured at point $P1$. Top: Growth of the magnetic field as the impellers' rotation rate F is increased from 10 to 22 Hz. Bottom: Sketch of the geometry of the mean magnetic field; toroidal component of the magnetic field (red), poloidal component (blue). From [57] & [72] with permission from © 2007, 2008 The American Physical Society.

Measurements of the magnetic field are fairly well resolved in the radial direction but have been performed only at a few axial and azimuthal locations (see Figure 4 left). Thus, although we cannot record higher-order modes, we observe that the mean magnetic field involves a leading order dipolar component with its axis along the rotation axis, $\mathbf{B_P}$, together with a related azimuthal component $\mathbf{B}_\theta$ (see Figure 5 right).

The amplitude of the magnetic field as a function of the magnetic Reynolds number is displayed in Figure 6. R_m has been defined as $R_m = K\mu_0\sigma R^2\Omega$ where R is the radius of the cylinder and Ω the rotation rate of the discs. $K = 0.6$ is a numerical coefficient relating ΩR to the maximum velocity in the flow. With this definition the critical magnetic Reynolds number is close to 31 as can be seen from Figure 6 (left) when the discs are rotated such that the leading edge of the

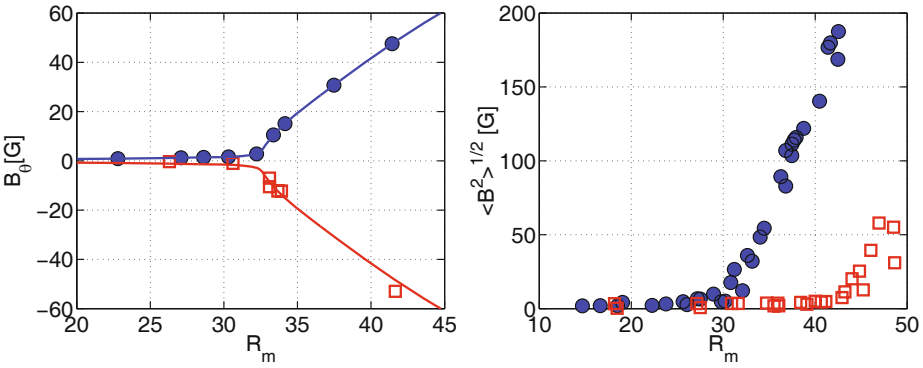

FIGURE 6. Left: Two independent realizations at same frequency above threshold showing opposite field polarities. Right: Magnetic field amplitude $\langle B^2 \rangle^{1/2} = \sqrt{B_x^2 + B_y^2 + B_z^2}$ at $P3$. Impellers are counterrotating at equal rotation rates, in the positive direction shown in Figure 4 (closed blue circles) or in the opposite direction, *i.e.*, with the blades on the impellers moving in a "scooping" or negative direction (open red squares). From [58] with permission from © 2009 AIP Publishing LLC.

curved blades is the convex one. The threshold is higher for the other direction (see Figure 6 right). Note that the two polarities of the magnetic field can be observed.

4.3. A possible dynamo mechanism for the VK flow

The mean VK flow has the following characteristics: the fluid is ejected radially outward by the discs; this drives an axial flow toward the discs along their axis and a recirculation in the opposite direction along the cylinder lateral boundary. In the case of counter-rotating impellers, the presence of a strong axial shear of azimuthal velocity in the mid-plane between the impellers generates a high level of turbulent fluctuations, roughly of the same order as the mean flow. It is thus unlikely that the fluctuations $\tilde{\mathbf{v}}$ can be neglected compared to $\overline{\mathbf{V}}$ in (1). It has been indeed observed that when the discs counter-rotate with the same frequency, a mean magnetic field is generated with a dominant axial dipolar component. Such an axisymmetric mean field cannot be generated by the mean flow alone, $\overline{\mathbf{V}}(r, x)$, that would give a non axisymmetric magnetic field according to Cowling theorem (Moffatt 1978). Non axisymmetric fluctuations $\tilde{\mathbf{v}}(r, \theta, x)$ thus play an essential role. As explained by Pétrélis *et al.* (2007), a possible mechanism is of $\alpha - \omega$ type, the α-effect being related to the helical motion of the radially expelled fluid between two successive blades of the impellers, and the ω-effect resulting from differential rotation due to counter-rotation of the impellers. This has been modeled using mean field MHD with an ad hoc α-effect related to this helical motion (Laguerre *et al.* 2009). The $\alpha - \omega$ mechanism has been illustrated without using mean field MHD by Gissinger (2009). When only the mean field velocity is taken into account

in a numerical simulation of the induction equation, the generated magnetic field is an equatorial dipole as displayed in Figure 7 (left) and observed earlier in several numerical works (Marié *et al.* 2003, Bourgoin *et al.* 2004, Ravelet *et al.* 2005, Stefani *et al.* 2006). When a non axisymmetric velocity component that mimics helical flow along the blades is taken into account, it is found that an axial dipole becomes the preferred growing mode (see Figure 7 right) in agreement with the VKS experiment. Thus, the VKS dynamo is not generated by the mean flow alone in contrast to Karlsruhe and Riga experiments, and non-axisymmetric fluctuations play an essential role in the dynamo process.

FIGURE 7. Geometry of the dynamo mode obtained by kinematic numerical simulations: (Left) an equatorial dipole is generated by the mean flow alone. (Right) When a non axisymmetric velocity component is taken into account, an axial dipole is generated. From [32] with permission from © 2009 IOP Publishing.

Another very important experimental fact is that the VKS dynamo has been observed so far only when impellers made of soft iron have been used. More precisely, one impeller at least should be made of soft iron and, it should be the rotating one if one of the impellers is at rest. It has been shown that magnetic boundary conditions corresponding to the high permeability limit significantly decrease the dynamo threshold (Gissinger *et al.* 2008, Gissinger 2009). However, it has been also claimed that other mechanisms could play a role: coupling with the magnetization inside the discs (Pétrélis *et al.* 2007), a possible additional source of ω-effect (Verhille *et al.* 2010) and the effect of a spatially periodic magnetic permeability along the azimuthal direction related to the blades (Giesecke *et al.* 2010). The later is the only one that has been simulated and found to decrease the

dynamo threshold further. However, recent experiments have shown that a spatially periodic magnetic permeability alone is not enough to generate a dynamo, thus these simulations deserve to be checked.

The essential role of ferromagnetic blades (in addition to ferromagnetic discs) can be also explained using the following simple argument: any azimuthal magnetic field is refracted when it hits the blades and channeled inside each blade. It is conveyed along the blades and should emerge near the center with an axial component in order to satisfy $\nabla \cdot \mathbf{B} = \mathbf{0}$. According to this simple mechanism, ferromagnetic blades convert some azimuthal field component into the poloidal one and thus provide some additional contribution to the α-effect.

4.4. Dynamics of the magnetic field in the VKS experiment

As said above, the magnetic field generated by impellers counter-rotating at the same speed is statistically stationary. No secondary bifurcation is observed up to the maximum possible speed allowed by the available motor power. The dynamics are much richer when the impellers are rotated at different speed as displayed by the parameter space (see Figure 8).

Different dynamical regimes are observed when, starting from impellers rotating at 22 Hz, the frequency of an impeller, say F_2, is decreased, F_1 being kept

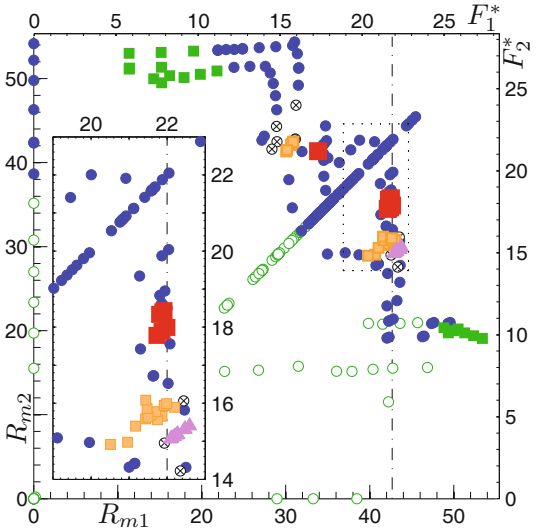

FIGURE 8. Dynamo regimes observed when the rotation frequencies F_1 and F_2 of the impellers are varied: no dynamo (green ○; $B \lesssim 10$G for more than 180 s), statistically stationary dynamos (blue ●); oscillatory dynamos (green squares); limit cycles (red squares), magnetic reversals (orange squares), bursts (purple triangles) and transient magnetic extinctions (⊗). From [72] with permission from © 2008 The American Physical Society.

constant. As said above, we first observe a statistically stationary dynamo regime with a dominant azimuthal mean field close to the flow periphery (see Figure 9, top left). This corresponds to the trace labelled 22–22 in the (B_r, B_θ) plane of Figure 9 (middle). As the frequency of the slower impeller is decreased, we obtain other stationary dynamo regimes for which the radial component of the mean field increases and then becomes larger than the azimuthal one (22–20 and 22–19). When we tune the impeller frequencies to 22 and 18.5 Hz respectively, a global bifurcation to a limit cycle occurs. We observe that the trajectory of this limit cycle goes through the location of the previous fixed points related to the stationary regimes. Direct time-recordings of the magnetic field, measured at the periphery of the flow in the mid-plane between the two impellers, are displayed in Figure 9 (bottom). We propose to ascribe the strong radial component (in green) that switches between ± 25 G to a quadrupolar mode (see Figure 9, top right). Its interaction with the dipolar mode that is the dominant one for exact counter-rotation, gives rise to the observed relaxation dynamics. The relaxation oscillation is observed in a rather narrow range of impeller frequency F_2 (less than 1 Hz). When the frequency of the slowest impeller in decreased further, statistically stationary regimes are recovered (22–18 to 22–16.5 Hz in Figure 9, middle). They also correspond to fixed points located on the trajectory of the limit cycle, except for the case 22–16.5 Hz that separates from it.

When the rotation frequency of the slowest impeller is decreased further, new dynamical regimes occur. One of them consists in field reversals (Berhanu *et al.* 2007). The three components of the magnetic field reverse at random intervals (Figure 10, left). The average length of phases with given polarity is two orders of magnitude larger than the duration of a reversal that corresponds to an ohmic diffusion time scale ($\tau_\sigma = \mu_0 \sigma L^2 \sim 1$ s on the scale L of the experiment). We emphasize that the trajectories connecting the $\mathbf{B}$ and $-\mathbf{B}$ states are robust despite the strong fluctuations of the flow. This is displayed in Figure 10 (right): the time evolution of reversals from up to down states can be superimposed by shifting the origin of time such that $\mathbf{B}(t = 0) = 0$ for each reversal. Down-up reversals are superimposed in a similar way on up-down ones by plotting $-\mathbf{B}$ instead of $\mathbf{B}$. The time evolution averaged on 12 successive reversals can be represented as the trajectory of the system in phase space using a plot of $[B_\theta(t), B_\theta(t - \delta t)]$ where $\delta t = 1$ s $\sim \tau_\sigma$ (see Figure 11). For each reversal, the field first decays exponentially with a rate 0.8 s^{-1}. The system then moves on a faster time scale to reach the state with opposite polarity after displaying an overshoot in the direct time recording (Figure 10, right). In phase space, this is related to the fact that the trajectory has to circle around each fixed point in order to reach it. The trajectory in phase space is amazingly robust despite strong velocity fluctuations. These fluctuations put an upper bound on the duration of phases with a given polarity. However, this does not suppress the scale separation between the length of the phases with given polarity and the duration of a reversal. In that sense, turbulent fluctuations have a weak effect on the large scale dynamics of the magnetic field.

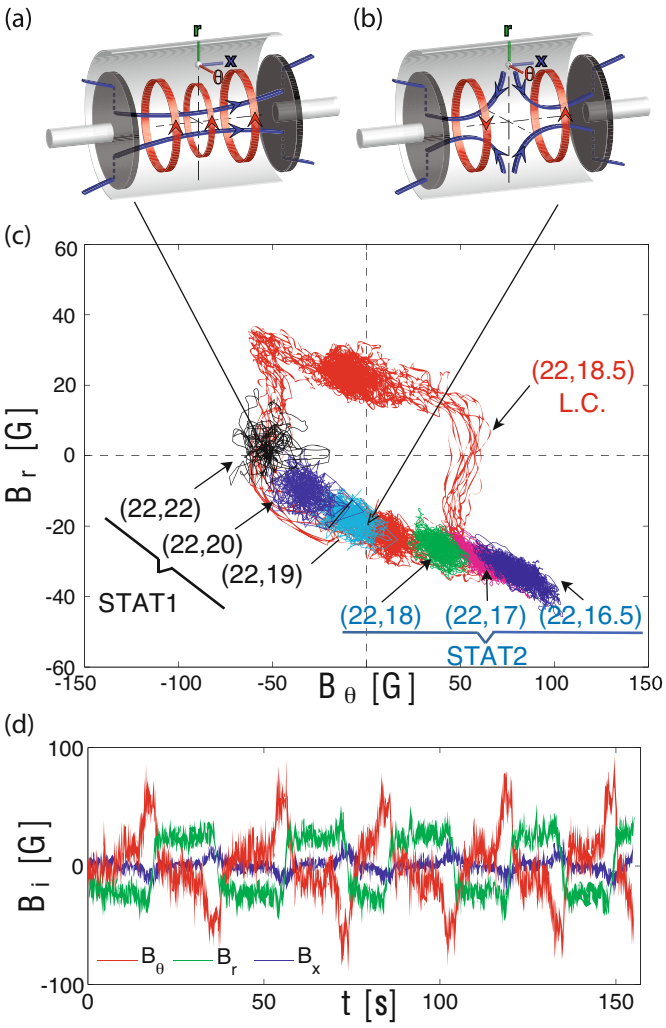

FIGURE 9. Sketch of the axial dipolar (a) and quadrupolar (b) magnetic modes. (c) location of the different states in the (B_r, B_θ) plane: fixed points corresponding to the stationary regimes for frequencies (F_1, F_2); limit cycle (L.C.) observed for impellers counterrotating at different frequencies $(22, 18.5)$Hz (red). The magnetic field is time averaged over 1 s to remove high frequency fluctuations caused by the turbulent velocity fluctuations. (d) time recording of the components of the magnetic field for frequencies $(22, 18.5)$Hz. From [58] with permission from © 2009 AIP Publishing LLC.

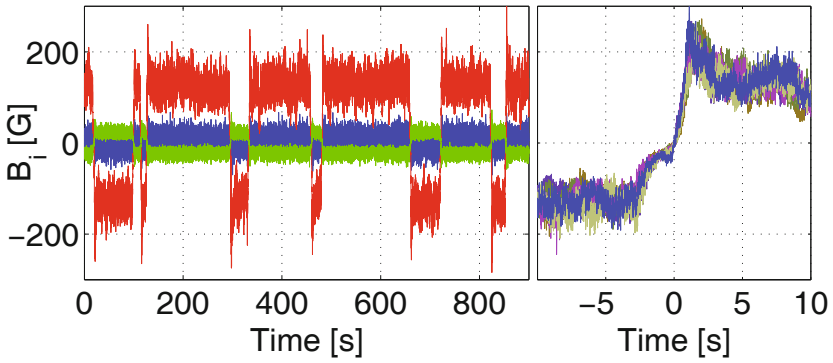

FIGURE 10. Reversals of the magnetic field generated by driving the flow with counterrotating impellers at frequencies $F_1 = 16$ Hz and $F_2 = 22$ Hz. Left: Time recording of the three magnetic field components at $P2$: axial (x) in blue, azimuthal (y) in red and radial (z) in green. Right: Superimposition of the azimuthal component for successive reversals from negative to positive polarity together with successive reversals from positive to negative polarity with the transformation $B \to -B$. For each of them the origin of time has been shifted such that it corresponds to $B = 0$. From [5] with permission from © 2009 AIP Publishing LLC.

When the magnetic field amplitude starts to decrease, either a reversal occurs, or the magnetic field first decays and then grows again with its direction unchanged. Similar sequences, called excursions, are also observed in recordings of the Earth's magnetic field. The phase space representation of Figure 11 is very appropriate to display them. One observes that the trajectory of an excursion is first similar to the one of reversals during their slow phase.

Other dynamical regimes are displayed in Figure 12. First, it is shown that there is a continuous transition from random reversals to noisy periodic behavior (top left and right) without any modification of the mechanical driving of the flow. Only the sodium temperature, and thus the Reynolds numbers are varied. Since the kinetic Reynolds number of the flow is very large, it is unlikely that its variation strongly affects the large scale flow. Observing nearly periodic oscillations rules out the naive picture in which reversals would only result from turbulent fluctuations driving the system away from a metastable state. For rotation frequencies 22–15 Hz, the magnetic field displays intermittent bursts (Figure 12, bottom right). The most probable value of the azimuthal field is roughly 20 G but bursts up to more than 100 G are observed such that the probability density function of the field has an exponential tail (not shown). For rotation frequencies 21–15 Hz, the same type of dynamics occur, but in a symmetric fashion, both positive and negative values of the field being observed (bottom left).

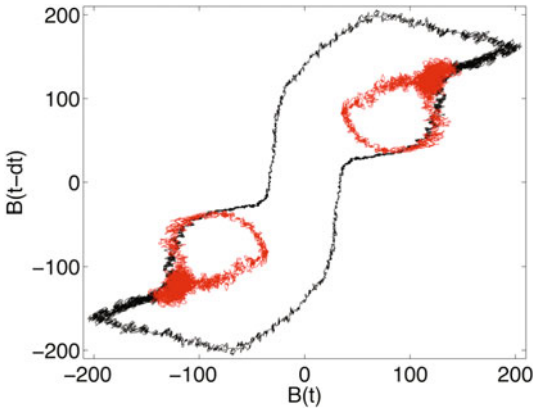

FIGURE 11. Plot of a planar cut of the phase space $[B_\theta(t), B_\theta(t-\delta t)]$ where $\delta t = 1$ s. The thick dots correspond to the two polarities of the magnetic field in its nearly stationary phases. The trajectories of reversals are represented in black. One excursion (together with the symmetric one) is represented in red. From [8], courtesy of E. Dormy, with permission from © 2007 IOP Publishing.

The different dynamical regimes of the magnetic field generated by the VKS flow display several characteristic features of low-dimensional dynamical systems. These dynamics will be understood below as the ones resulting from the competition between a few nearly critical modes. We emphasize that what is remarkable in these experiments is the robustness of these low-dimensional dynamical features that are not smeared out despite large turbulent fluctuations of the flow that generates the dynamo field.

5. Low-dimensional models of field reversals

It has been known since the work of Brunhes (1906) that Earth's magnetic field remains roughly parallel to the same direction, almost its rotation axis, for long durations (100000 years or much longer) but from time to time, it flips with the poles reversing sign. Polarity reversals are also observed for the magnetic field of the sun. Both its large scale dipolar component as well as the intense concentrations of magnetic field observed at smaller scales in the sun spots reverse sign roughly every 11 years.

Flows in the interiors of planets or stars have huge kinetic Reynolds numbers. For instance, $Re \sim 10^9$ in the Earth's liquid core or $Re \sim 10^{15}$ in the convective zone of the Sun. These flows being strongly turbulent, we would expect them to advect and distort the magnetic field lines in a very complicated way both in space and time. Thus, it is puzzling that the generated magnetic fields display a large

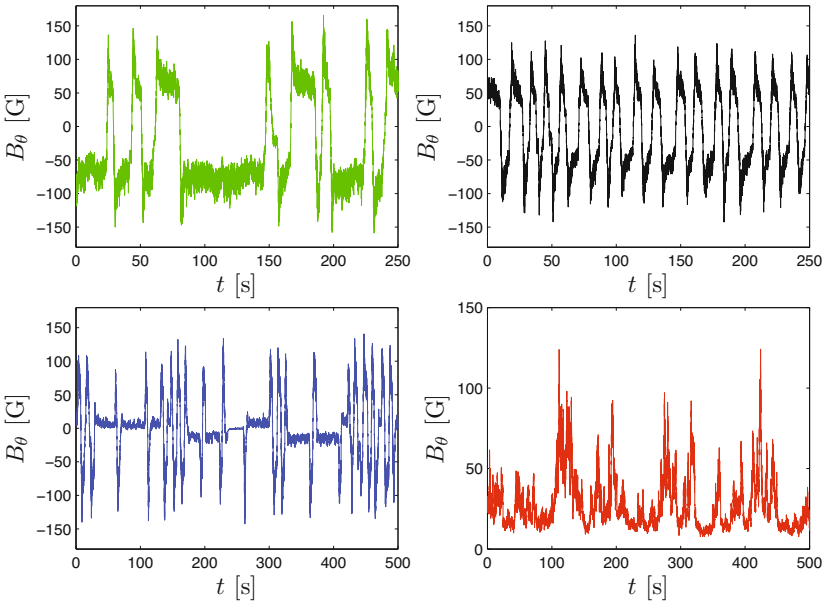

FIGURE 12. Top: Time recordings of the azimuthal component of the magnetic field observed for impellers rotating at (22–16) Hz. The sodium temperature is 131° C (left) and 147° C (right). Bottom: Time recordings of the azimuthal component of the magnetic field observed for impellers rotating at (22–15) Hz (left), (21–15) Hz (right). From [72] with permission from © 2008 The American Physical Society.

scale coherent component with rather simple dynamics: a dominant dipolar component, roughly aligned with the rotation axis for Earth and an oscillatory magnetic field with well-characterized spatial features for the sun (Zeldovich *et al.* 1983).

As just described, qualitatively similar dynamics have been observed in the VKS experiment. We will first shortly review the different models that have been proposed for the dynamics of the magnetic fields of the Earth and the Sun. Then, we will present in Section 6 a simple model of the dynamics observed in the VKS experiment.

5.1. Disc dynamos and truncations of the MHD equations

The first simple models of field reversals involved couple rotor disc dynamos (Rikitake 1958, Allan 1962, Cook and Roberts 1970) or even a Bullard disc dynamo when a shunt is added (Malkus 1972, Robbins 1977). The equations for the currents are of same type as Lorenz model (Lorenz 1963). When the two solutions $\pm I_0$ related one to the other by the $B \to -B$ symmetry are unstable and chaotic regimes occur, these systems stay for a while in the vicinity of one solution and then

flips to the neighborhood of the other. These transitions occur in a random fashion and this can be considered as reversal dynamics. However, both the shape of the transitions displayed by direct recordings or in the phase space as well as their statistical properties differ from the experimental observations of field reversals and from paleomagnetic records. In addition, equations governing disc dynamos strongly differ from full MHD equations and cannot be obtained from them in any consistent approximation. It is however possible to relate Rikitake equations with a simple model of an $\alpha - \omega$ dynamo (Moffatt 1978). It has been also shown by Nozières (1978) that equations similar to the ones of disc dynamos can be obtained by truncating the full MHD equations. Keeping two magnetic modes of the diffusion operator and one velocity mode, equations similar (but not identical) to Rikitake (1958) are found. Nozières then describe reversals as a relaxation limit cycle between two quasi-stationary states related by the $B \to -B$ symmetry.

The main problem with truncated systems is that they usually describe dynamics that do not persist when higher modes are taken into account. The most famous example is the Lorenz attractor (Lorenz 1963) obtained from a drastic truncation of a Rayleigh–Bénard convection problem. Although its discovery has been one of the major steps of dissipative dynamical system theory and triggered a lot of studies, its chaotic dynamics does not subsist when higher modes of the convection problem are kept. The dynamo problem is even more sensitive to truncation. The growth of the magnetic field itself can result from a truncation of the velocity field even when a fair enough number of modes are kept whereas no dynamo exists when the resolution is good enough. It seems therefore unlikely that truncated systems involving a few coupled velocity and magnetic modes would correctly describe reversals of the magnetic field.

5.2. Normal forms

A different class of models, also involving a few coupled differential equations, is based on the assumption that several magnetic eigenmodes are competing above the dynamo threshold. These models have been mostly used in the context of low-order stellar dynamo models and more particularly to describe the solar cycle and its slow modulation. Tobias *et al.* (1995) take into account two magnetic modes (a poloidal and a toroidal one) undergoing a Hopf bifurcation in the framework of Parker's model (Parker 1955). They assume that the velocity field generating the magnetic field is close to a saddle-node bifurcation and couple the marginal velocity mode to the magnetic modes in order to obtain a third-order system which displays periodic, quasiperiodic and chaotic behaviours when the system parameters are varied. Wilmot-Smith *et al.* (2005) obtain similar results but with a coupling term that does not break the $B \to -B$ symmetry.

Knobloch & Landsberg (1996) consider a different model that does not involve marginal velocity modes but two magnetic modes, a dipolar and a quadrupolar one, both generated through a Hopf bifurcation. Taking into account $1:1$ resonant coupling terms, they find aperiodic regimes that can also represent the modulation of the cyclic activity of the solar magnetic field. Finally, Knobloch *et al.* (1998)

assume the existence of two velocity modes, symmetric (respectively antisymmetric) with respect to the equatorial plane, and couple them to the dipolar and quadrupolar magnetic modes of the previous model. They show that two different types of modulation of the cyclic activity can be described.

In the framework of normal forms, it has been proposed to relate reversals to trajectories close to heteroclinic cycles that connect unstable fixed points $\pm\mathbf{B}$ (Armbruster *et al.* 2001, Chossat & Armbruster 2003). Heteroclinic cycles provide a simple framework to describe separation of time scales between quasi-steady states with a given polarity, related to the slowing down of the system in the vicinity of a saddle point, and rapid reversal events. Heteroclinic cycles are generally structurally unstable except in the presence of symmetries that lead to invariant subspaces of the dynamical system. Melbourne *et al.* (2001) try to describe the dynamics of Earth's magnetic field by writing amplitude equations for an equatorial dipole coupled to axial dipole and quadrupole. This model has heteroclinic cycles but no connection of states with opposite polarities except when additional coupling terms that break the symmetries are taken into account. Strictly speaking, a stable heteroclinic cycle connecting $\pm\mathbf{B}$ cannot describe reversals because the period of the trajectory in phase space goes to infinity as the trajectory is attracted on the cycle. However, an arbitrary amount of noise is enough to kick the system away from the saddle points and to generate random reversals with a finite mean period (Stone & Holmes 1990).

5.3. Metastable states in the presence of external noise

Other models rely on external noise in a stronger way. They start from a dipolar magnetic mode with amplitude $D(t)$ that bifurcates supercritically and model the effect of hydrodynamic turbulence through random fluctuations of the coefficients of the dynamical system governing D and the amplitudes of the stable modes in the vicinity of the bifurcation threshold. Fluctuations only in the amplitude equation, $\dot{D} = \mu D - D^3$, i.e., a growth rate μ that involves a noisy component, does not lead to reversals between the two stationary solutions $D = \pm\sqrt{\mu}$. However, taking into account that D is coupled with the amplitudes of the stable modes which are also excited by fluctuations, can lead to reversals (Schmitt *et al.* 2001). D behaves as the position of a strongly damped particle driven by random noise in a two-well potential. The crucial role of damped modes has been emphasized further by Hoyng & Duistermaat (2004). The reversals are triggered by large fluctuations of damped modes driven by noise. These modes act on D as an effective additive noise.

Recent numerical simulations have modelled hydrodynamic fluctuations with a noisy α-effect (Giesecke *et al.* 2005, Stefani & Gerbeth 2005, Stefani *et al.* 2007). The deterministic part of this model can generate periodic relaxation oscillations with the system slowing down in the vicinity of two states with opposite polarities $\pm\mathbf{B}$. In this respect, it belongs to the class of systems described by Nozières (1978). The addition of external noise is thus crucial to generate random reversals. It is likely that the phenomenology of this model is related to the proximity of

a codimension-two point that results from two interacting modes with different radial structures.

5.4. Hydrodynamic mechanisms and direct numerical simulations

The above descriptions of reversals assume the existence of some large scale dominant modes of the magnetic field. The random dynamics of reversals are either of deterministic nature (low-dimensional chaos) or result from the addition of external noise that describes hydrodynamic fluctuations.

A different approach, initiated by Parker (1969), consists in trying to identify the nature of the fluctuations of the velocity field that is required to generate a reversal. In the case of Earth, it is believed that the magnetic field is generated through an α-ω mechanism, ω being related to differential rotation and α resulting from the existence of a mean number of cyclonic convective cells in Earth's core, that fluctuate both in number and position. When strong enough, these fluctuations can reverse the magnetic field (Parker 1969, Levy 1972).

Another mechanism has been also proposed by Parker (1979). It follows from the observation by Roberts (1972) that a meridional circulation favors stationary dipolar α-ω dynamos in spherical geometries. Parker (1979) suggested that if the meridional circulation is altered for a while, an oscillatory magnetic mode may become dominant and generates a reversal of the magnetic field. It has been claimed later that this mechanism can be also suggested from palaeomagnetic data (McFadden & Merrill 1995). Numerical simulations of the MHD equations in a rotating sphere have displayed this in a clear-cut way: it has been shown by Sarson & Jones (1999) and Sarson (2000) that the random emission of poleward light plumes, or "buoyancy surge", generates fluctuations of the meridional flow that can trigger a reversal. They also found that this mechanism is not affected much by the back reaction of the magnetic field on the flow and does result from the proximity in parameter space of stationary and time periodic dynamo modes, depending on the intensity of the meridional flow. A process also related to convective plumes has been observed by Wicht & Olson (2004). They found that a magnetic field with an opposite polarity is produced locally in the convective plumes and that the transport of this reversed flux can generate a reversal. They also showed that the observed reversals are almost unchanged when the Lorentz force is removed from the numerical code. Other advection processes of the magnetic field by the flow have been studied in detail by Aubert *et al.* (2008). It should be noted that all these numerical simulations have been performed with large values of P_m ($1 < P_m < 20$). Local modifications of the magnetic field by the flow are likely to play a less important role for small values of P_m because they are strongly damped by ohmic diffusion.

Since 1995 (Glatzmaier & Roberts 1995), a lot of three-dimensional numerical simulations of the MHD equations in a rotating sphere have been able to simulate a self-consistent magnetic field that displays reversals (see the reviews by Dormy *et al.* 2000, Roberts & Galtzmaier 2000). However, it has been emphasized that most relevant dimensionless parameters that can be achieved in direct simulations

are orders of magnitude away from their value in Earth's core or laboratory experiments. Even in the limited range accessible to direct simulations, it has been shown that the geometry of the generated magnetic field and the properties of field reversals can strongly depend on the values of the relevant dimensionless numbers (Kutzner & Christensen 2002, Busse & Simitev 2006). Thus, one may conclude as in Coe *et al.* (2000) that "each reversal in the simulations has its own unique character, which can differ greatly in various aspects from others". However, we emphasize that a lot of these numerical simulations also display similar properties at a more global level, if one considers the how the symmetries of the flow and the magnetic field evolve during a reversal. We will discuss this aspect in the next section.

6. A simple model for the dynamics observed in the VKS experiment

The most striking feature of the VKS experiment is that time dependent magnetic fields are generated only when the impellers rotate at different frequencies (Berhanu *et al.* 2007, Ravelet *et al.* 2008). We have shown in Pétrélis & Fauve (2008) that this is related to the additional invariance under $\mathcal{R}_\pi$ when $F_1 = F_2$ (rotation of an angle π along any axis in the mid-plane). We indeed expect that in that case, the modes involved in the dynamics are either symmetric or antisymmetric. Such modes are displayed in Figure 13. A dipolar mode is changed to its opposite by $\mathcal{R}_\pi$, whereas a quadrupolar mode is unchanged.

We assume that the magnetic field is the sum of a dipolar component with an amplitude D and a quadrupolar one, Q. We define $A = D + i\,Q$ and we assume that an expansion in power of A and its complex conjugate $\bar{A}$ is pertinent close to threshold in order to obtain an evolution equation for both modes. Taking into

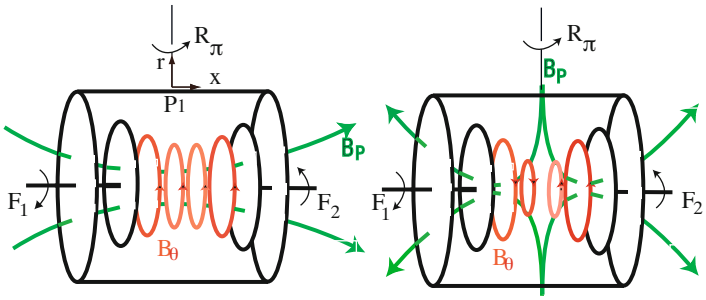

FIGURE 13. Possible eigenmodes of the VKS experiment. The two discs counter-rotate with frequency F_1 and F_2. Left: Magnetic dipolar mode. Right: Magnetic quadrupolar mode. Poloidal (green) and toroidal (red) components are sketched.

account the invariance $\mathbf{B} \to -\mathbf{B}$, i.e., $A \to -A$, we obtain

$$\dot{A} = \mu A + \nu \bar{A} + \beta_1 A^3 + \beta_2 A^2 \bar{A} + \beta_3 A \bar{A}^2 + \beta_4 \bar{A}^3 \,, \tag{8}$$

where we limit the expansion to the lowest-order nonlinearities. In the general case, the coefficients are complex and depend on the experimental parameters.

Symmetry of the experiment with respect to $\mathcal{R}_\pi$ when the discs exactly counter-rotate, amounts to constraints on the coefficients. Applying this transformation to the magnetic modes, changes D into $-D$ and Q into Q, thus $A \to -\bar{A}$. We conclude that, in the case of exact counter-rotation, all the coefficients are real. When the frequency difference $f = F_1 - F_2$ is increased from zero, we obtain that the real parts of the coefficients are even and the imaginary parts are odd functions of f. When the coefficients are real, the growth rate of the dipolar component is $\mu_r + \nu_r$ and that of the quadrupolar component is $\mu_r - \nu_r$. The dipole being observed for exact counter-rotation implies that $\nu_r > 0$ for $f = 0$. By increasing f, we expect that ν_r changes sign and favors the quadrupolar mode according to the experimental results (see Figure 9). We will explain in the next section how modifying the parameters of (8) leads to bifurcation to time dependent solutions.

6.1. A mechanism for oscillations and reversals

As shown in Pétrélis & Fauve (2008), the planar system (8) explains the dynamical regimes observed so far in the VKS experiment (Ravelet *et al.* 2008). It is invariant under the transformation $\mathbf{B} \to -\mathbf{B}$. Thus, in the case of counter-rotating impellers, $F_1 = F_2$, it has two stable dipolar solutions $\pm D$ and two unstable quadrupolar solutions $\pm Q$. When the frequency difference f is increased, these solutions become more and more mixed due to the increase of the strength of the coupling terms between dipolar and quadrupolar modes. Dipolar (respectively quadrupolar) solutions get a quadrupolar (respectively dipolar) component and give rise to the stable solutions $\pm B_s$ (respectively unstable solutions $\pm B_u$) displayed in Figure 14. When f is increased further, a saddle-node bifurcation occurs, i.e., the stable and unstable solutions collide by pairs and disappear. This generates a limit cycle that connects the collision point with its opposite. This result can be understood as follows: the solution $B = 0$ is unstable with respect to the two different fixed points, and their opposite. It is an unstable point, whereas one of the two bifurcating solutions is a stable point, a node, and the other is a saddle. If the saddle and the node collide, say at B_c, what happens to initial conditions located close to these points? They cannot be attracted by $B = 0$ which is unstable and they cannot reach other fixed points since they just disappeared. Therefore the trajectories describe a cycle. The associated orbit contains $B = 0$ since, for a planar problem, in any orbit, there is a fixed point. Suppose that the orbit created from B_c is different from the one created by $-B_c$. These orbits being images by the transformation $\mathbf{B} \to -\mathbf{B}$, they must intersect at some point. Of course, this is not possible for a planar system because it would violate the uniqueness of the solutions. Therefore, there is only one cycle that connects points close to B_c and $-B_c$.

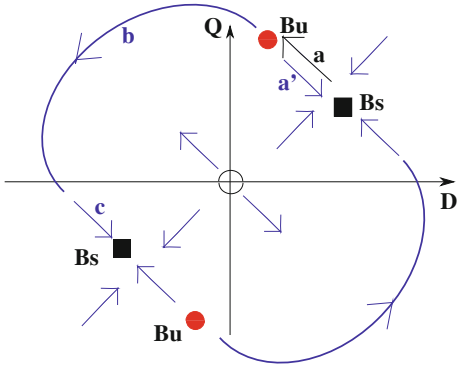

FIGURE 14. A generic saddle-node bifurcation in a system with the $\mathbf{B} \to -\mathbf{B}$ invariance: below threshold, fluctuations can drive the system against its deterministic dynamics (phase a). If the effect of fluctuations is large enough, this generates a reversal (phases b and c). Otherwise, an excursion occurs (phase a′). From [68] with permission from © 2008 IOP Publishing.

This provides an elementary mechanism for field reversals in the vicinity of a saddle-node bifurcation. First, in the absence of fluctuations, the limit cycle generated at the saddle-node bifurcation connects $\pm B_c$. This corresponds to periodic reversals. Slightly above the bifurcation threshold, the system spends most of the time close to the two states of opposite polarity $\pm B_c$. Second, in the presence of fluctuations, random reversals can be obtained slightly below the saddle-node bifurcation. B_u being very close to B_s, even a fluctuation of small intensity can drive the system to B_u from which it can be attracted by $-B_s$, thus generating a reversal.

The effect of turbulent fluctuations on the dynamics of the two magnetic modes governed by (8) can be easily modeled by adding some noisy component to the coefficients (Pétrélis & Fauve 2008). Random reversals are displayed in Figure 15 (top left). The system spends most of the time close to the stable fixed points $\pm B_s$. We observe in Figure 15 (top right) that a reversal consists of two phases. In the first phase, the system evolves from the stable point B_s to the unstable point B_u (in the phase space sketched in Figure 14). The deterministic part of the dynamics acts against this evolution and the fluctuations are the motor of the dynamics. That phase is thus slow. In the second phase, the system evolves from B_u to $-B_s$, the deterministic part of the dynamics drives the system and this phase is faster.

The behaviour of the system close to B_s depends on the local flow. Close to the saddle-node bifurcation, the position of B_s and B_u defines the slow direction of the dynamics. If a component of B_u is smaller than the corresponding one of B_s, that component displays an overshoot at the end of a reversal. In the opposite case, that component will increase at the beginning of a reversal. For instance, in

the phase space sketched in Figure 14, the component D decreases at the end of a reversal and the signal displays an overshoot. The component Q increases just before a reversal.

For some fluctuations, the second phase does not connect B_u to $-B_s$ but to B_s. It is an aborted reversal or an excursion in the context of the Earth dynamo. Note that during the initial phase, a reversal and an excursion are identical. In the second phase, the approaches to the stationary phase differ because the trajectory that links B_u and B_s is different form the trajectory that links B_u and $-B_s$. In particular, if the reversals display an overshoot this will not be the case of the excursion (see Figure 15 top right) and the sketch of the cycle in Figure 14).

Finally, it is illustrated in Figure 15 (bottom left and right), that the other dynamical regimes of the VKS experiment, such as symmetric or asymmetric intermittent bursts, can be described with the same model (Pétrélis & Fauve 2008).

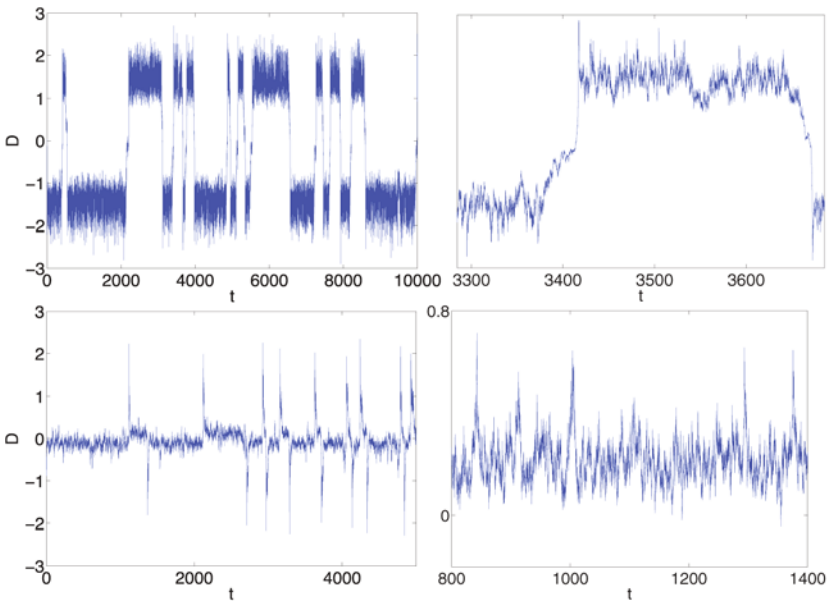

FIGURE 15. Time recordings obtained from equation (8) displaying different dynamics of the magnetic field, as observed in the VKS experiment: reversals, symmetric bursts and asymmetric bursts. From [68] with permission from © 2008 IOP Publishing.

6.2. A simple model for Earth's magnetic field reversals

The above model of reversals of magnetic field in the vicinity of a saddle-node bifurcation in a system with the invariance $\mathbf{B} \to -\mathbf{B}$ explains many intriguing features of the reversals of Earth magnetic field (Pétrélis *et al.* 2009). The most

significant output is that the mechanism predicts specific characteristics of the field obtained from paleomagnetic records (Valet *et al.* 2005), in particular their asymmetry: the Earth's dipole decays on a slower time scale than it recovers after a reversal. In addition, it displays an overshoot that immediately follows the reversals. Other characteristic features such as excursions as well as the existence of superchrons are understood in the same framework.

Although the symmetries of the flow in the Earth's core strongly differ from the ones of the VKS experiment, dipolar and quadrupolar modes can be defined with respect to equatorial symmetry such that model (8) can be transposed for Earth's magnetic field. From an analysis of paleomagnetic data, it has been proposed that reversals involve an interaction between dipolar and quadrupolar modes (McFadden *et al.* 1991). We thus obtain an interesting prediction about the liquid core in that case: if reversals involve a coupling of the Earth's dipole with a quadrupolar mode, then this requires that the flow in the core has broken mirror symmetry. In contrast, another scenario has been proposed in which the Earth's dipole is coupled to an octupole, i.e., another mode with a dipolar symmetry. This does not require additional constraint on the flow in the core in the framework of our model. In any case, the existence of two coupled modes allows the system to evolve along a path that avoids $\mathbf{B} = \mathbf{0}$. In physical space, this means that the total magnetic field does not vanish during a reversal but that its spatial structure changes.

7. Different morphologies for field reversals

We have shown in the previous section that an efficient way to reverse an axial dipolar field is to couple it with another mode. In the case of axisymmetric mean fields, an axial quadrupole is a natural choice. However, one can imagine that it can be also possible to involve a non-axisymmetric mode in the dynamics of reversals. In that case, the leading order choice would be an equatorial dipole. This type of scenario has been recently observed in numerical simulations of a flow driven by counter-rotating propellers in a spherical domain. This geometry displays many similarities with the one of the VKS experiment (in both cases, a cylindrical symmetry is related to the rotation axis). It corresponds to the Madison experiment. Although no dynamo has been observed yet, numerical simulations have been performed (Bayliss *et al.* 2007, Gissinger *et al.* 2008, 2010). In the case of counter-rotating propellers, an equatorial dipole is observed when the kinetic Reynolds number is small (Gissinger *et al.* 2008). However, for moderate kinetic Reynolds numbers, $Re \sim 300$, the flow involves fluctuations that drives an axial dipole first (see Figure 16).

As for the VKS experiment, this axial dipole displays reversals only when the $\mathcal{R}_\pi$ symmetry is broken by rotating the propellers at different speeds. In the simulations, this is achieved by multiplying the forcing by a parameter C, with $C = 1$ for the lower hemisphere but can be different from one for the upper

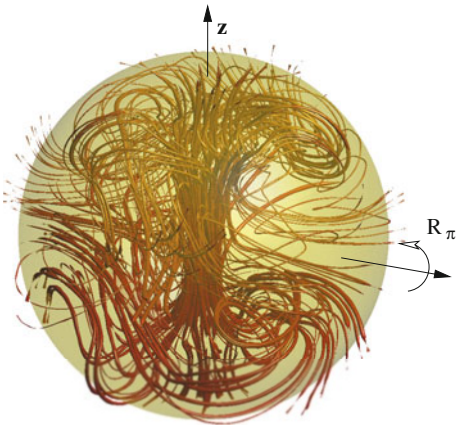

FIGURE 16. Magnetic field lines obtained with a symmetric forcing ($C = 1$) for $R_m = 300$ and $P_m = 1$. Note that the field involves a dipolar component with its axis aligned with the axis z of rotation of the propellers. From [33] with permission from © 2010 IOP Publishing.

one. Time recordings of some components of the magnetic field are displayed in Figure 17 for $R_m = 300$, $P_m = 1$ and $C = 2$. We observe that the axial dipolar component (in black) randomly reverses sign. The phases with given polarity are an order of magnitude longer than the duration of a reversal that corresponds to an ohmic diffusion time. The magnetic field strongly fluctuates during these phases because of hydrodynamic fluctuations. It also displays excursions. All of these

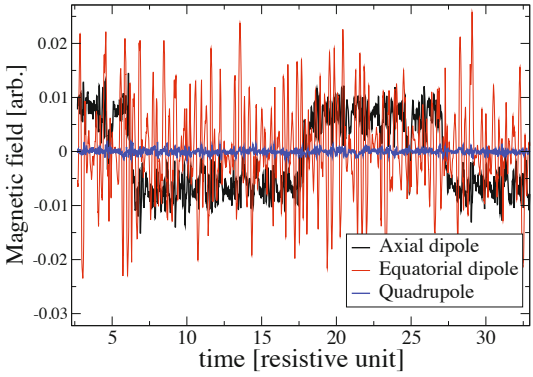

FIGURE 17. Time recording of the axial dipolar magnetic mode (in black), the axial quadrupolar mode (in blue) and the equatorial dipole (in red) for $R_m = 300$, $P_m = 1$ and $C = 2$. From [33] with permission from © 2010 IOP Publishing.

features are also observed in the VKS experiment. However, the simulation for $P_m = 1$ also displays strong differences with the VKS experiment. The equatorial dipole is the mode with the largest fluctuations whereas the axial quadrupolar component is an order of magnitude smaller than the dipolar modes. In addition, it does not seem to be coupled to the axial dipolar component.

We now turn to simulations using only smaller values of P_m (values comparable to the ones of the VKS experiment are out of reach in direct numerical simulations). The time evolution of the magnetic modes for $R_m = 165$, $P_m = 0.5$ and $C = 1.5$ is represented on Figure 18 (left). It differs significantly from the

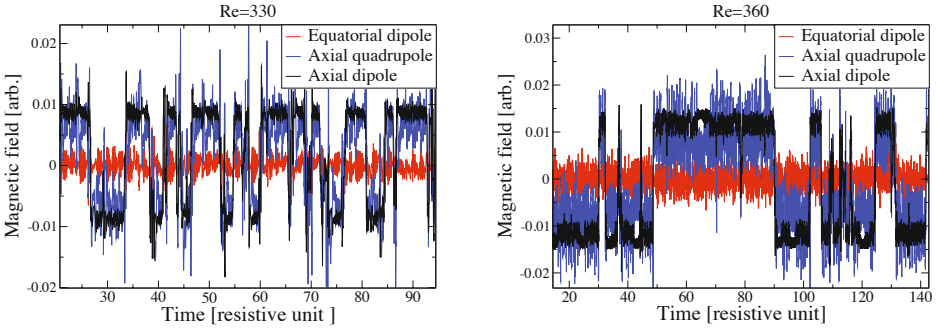

FIGURE 18. Time recordings of the axial dipole (black), the axial quadrupole (blue) and the equatorial dipole (red). Left: $R_m = 165$, $P_m = 0.5$ and $C = 1.5$. Right: $R_m = 180$, $P_m = 0.5$ and $C = 2$. From [33] with permission from © 2010 IOP Publishing.

previous case ($P_m = 1$). First of all, the quadrupole is now a significant part of the field, and reverses together with the axial dipole. The equatorial dipole remains comparatively very weak and unessential to the dynamics. One can argue that R_m has also been modified when changing P_m from 1 to 0.5. However, for $P_m = 1$, we have observed the same dynamics of reversals when R_m has been decreased down to $R_m = 220$ below which reversals are not observed any more.

The high amount of fluctuations observed in these signals is related to hydrodynamic fluctuations. One could be tempted to speculate that a higher degree of hydrodynamic fluctuations necessarily yields a larger reversal rate. Such is in fact not the case. A more sensible approach could be to try to relate the rate of reversals to the amount of fluctuations of the magnetic modes in a phase with given polarity. Increasing R_m from 165 to 180 does yield larger fluctuations as shown in Figure 18 (right). However the reversal rate is in fact lowered because C was modified to $C = 2$. This clearly shows that the asymmetry parameter C plays an important role in addition to the fluctuations of the magnetic field. For $P_m = 0.5$, reversals occur only in a restricted region, $1.1 < C < 2.5$, which is also a feature of the VKS experiment. The reversal rate strongly depends on the value of C with

respect to these borders, in good agreement with the model presented in Pétrélis & Fauve (2008). Thus, the transition from a stationary regime to a reversing one is not generated by an increase of hydrodynamic fluctuations.

We have thus shown that different types of random reversals of a dipolar magnetic field can be obtained by varying the magnetic Prandtl number in a rather small range around $P_m = 1$. This may be of interest for simulations of the magnetic field of the Earth that have been mostly restricted to values of P_m larger than one. We have observed that axisymmetric dipolar and quadrupolar modes decouple from the other magnetic modes while getting coupled together when P_m is decreased. Although we do not claim to have reached an asymptotic low P_m regime which is out of reach of the present computing power, we observe that dominant axial dipole and quadrupole are also observed in the VKS experiment for which $P_m \sim 10^{-5}$.

8. A minimal model for field reversals

These direct numerical simulations illustrate the role of the magnetic Prandtl number (or possibly of the distance to the dynamo threshold) in the dynamics of reversals. We now write the simplest dynamical system that involves the three modes that look important in the low P_m simulations: the dipole D, the quadrupole Q, and the zonal velocity mode V that breaks the $\mathcal{R}_\pi$ symmetry. These modes transform as $D \to -D$, $Q \to Q$ and $V \to -V$ under the $\mathcal{R}_\pi$ symmetry. Keeping nonlinear terms up to quadratic order, we get

$$\dot{D} = \mu D - VQ, \tag{9}$$

$$\dot{Q} = -\nu Q + VD, \tag{10}$$

$$\dot{V} = \Gamma - V + QD. \tag{11}$$

A non zero value of Γ is related to a forcing that breaks the $\mathcal{R}_\pi$ symmetry, i.e., propellers rotating at different speeds.

The dynamical system (9)–(11) with $\Gamma = 0$ occurs in different hydrodynamic problems and has been analyzed in detail (Hughes & Proctor 1990). The relative signs of the coefficients of the nonlinear terms have been taken such that the solutions do not diverge when $\mu > 0$ and $\nu < 0$. Their modulus can be taken equal to one by appropriate scalings of the amplitudes. The velocity mode is linearly damped and its coefficient can be taken equal to -1 by an appropriate choice of the time scale. Note that similar equations were obtained with a drastic truncation of the linear modes of MHD equations (Nozières 1978). However, in that context μ should be negative and the damping of the velocity mode was discarded, thus strongly modifying the dynamics.

This system displays reversals of the magnetic modes D and Q for a wide range of parameters. A time recording is shown in Figure 6. The mechanism for these reversals results from the interaction of the modes D and Q coupled by the broken $\mathcal{R}_\pi$ symmetry when $V \neq 0$. It is thus similar to the one described in

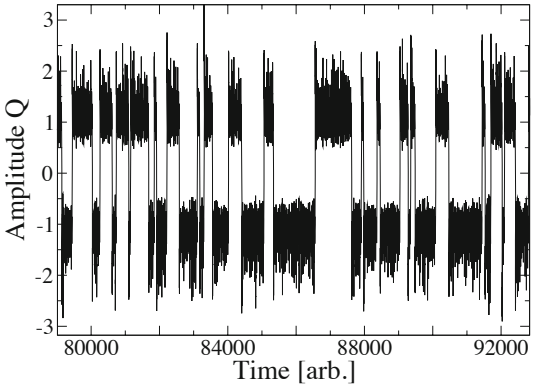

FIGURE 19. Numerical integration of the amplitude equations (9)–(11). Time recording of the amplitude of the quadrupolar mode for $\mu = 0.119$, $\nu = 0.1$ and $\Gamma = 0.9$. From [33] with permission from © 2010 IOP Publishing.

Section 6 but also involves an important difference: keeping the damped velocity mode into the system generates chaotic fluctuations. It is thus not necessary to add external noise to obtain random reversals. This system is fully deterministic as opposed to the one of Pétrélis and Fauve (2008). The phase space displayed in Figure 20 (left) shows the existence of chaotic attractors in the vicinity of the $\pm\mathbf{B}$ quasi-stationary states. When these symmetric attractors are disjoint, the magnetic field fluctuates in the vicinity of one of the two states $\pm\mathbf{B}$ and the dynamo

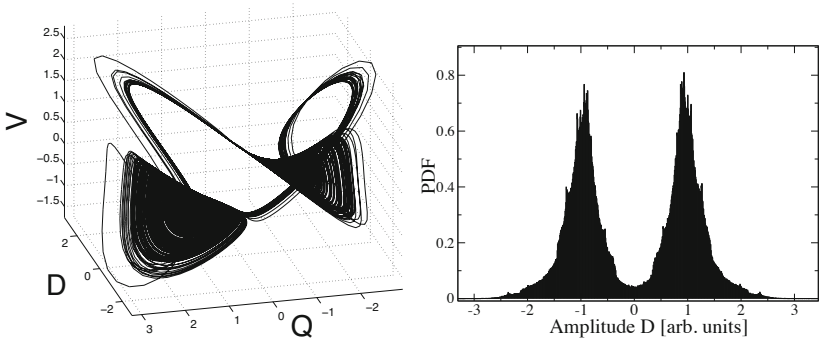

FIGURE 20. Numerical integration of the amplitude equations (9)–(11). Left: Three-dimensional phase space. Right: Probability density function of D ($\mu = 0.119$, $\nu = 0.1$ and $\Gamma = 0.9$). From [33] with permission from © 2010 IOP Publishing.

is statistically stationary. When μ is varied, these two attractors can get connected through a crisis mechanism, thus generating a regime with random reversals.

We do not claim that this minimal low-order system fully describes the direct simulations presented here. For instance, in the case of exact counter-rotation ($C = 1$, i.e., $\Gamma = 0$), equations (9)–(11) do not have a stable stationary state with a dominant axial dipole. The different solutions obtained when μ is increased cannot capture all the dynamo regimes of the VKS experiment or of the direct simulations when R_m is increased away from the threshold. Taking into account cubic nonlinearities provides a better description of the numerical results for $P_m = 0.5$. However, this three mode system with only quadratic nonlinearities involves the basic ingredients of the reversals observed in the present numerical simulations for low enough values of the magnetic Prandtl number. As recalled in Section 5, geomagnetic reversals have been modeled since a long time using low-dimensional dynamical systems or equations involving a noisy forcing. The above model (9)–(11) does not rely on an external noise source to generate random reversals. Compared to previous deterministic models, it displays dynamical and statistical properties that are much closer to the ones of our direct simulations at low P_m or of the VKS experiment. For instance, the direct recordings of D or Q do not involve the growing oscillations characteristic of reversals displayed by the Rikitake or Lorenz systems but absent in dynamo experiments or in direct simulations. Correspondingly, the probability density function of D displayed in Figure 20 (right) is also much closer to the one obtained in experiments or direct simulations than the one of previous deterministic models.

9. Conclusion

We have studied dynamical regimes that can arise when two axisymmetric magnetic eigenmodes are coupled. Symmetry considerations allow to identify properties of the magnetic modes and, in some cases, put constraints on the coupling between the modes. We have shown that when a discrete symmetry is broken by the flow that generates the magnetic field, the coupling between an odd and an even magnetic mode (with respect to the symmetry) can generate a bifurcation from a stationary state to a periodic state. This behaviour is generic when a saddle-node bifurcation occurs in a system that is invariant under $\mathbf{B} \to -\mathbf{B}$. Close to the bifurcation threshold, fluctuations drive the system into a state of random reversals that connect a solution B_s to its opposite $-B_s$. This scenario provides a simple explanation for many features of the dynamics of the magnetic field observed in the VKS experiment: alternation of stationary and time dependent regimes when a control parameter is varied, continuous transition from random reversals to time periodic ones, characteristic shapes of the time recordings of reversals versus excursions.

Although the discrete symmetry involved for the flow in the Earth core is different from the one of the VKS experiment, a similar analysis can be performed for the geodynamo (Pétrélis *et al.* 2009).

More generally, our scenario can be applied to purely hydrodynamic systems. Cellular flows driven by thermal convection (Krishnamurti & Howard 1981) or by volumic forces (Sommeria 1986) display a transition for which a large scale circulation is generated on a smaller scale turbulent background. This large scale flow can display random reversals, very similar to the ones observed for the magnetic field. A model analogue to the present one, can explain how this large scale field can reverse without the need of a very energetic turbulent fluctuation acting coherently in the whole flow volume.

Acknowledgment

I thank the members of the VKS team with whom the experimental data reported in Section 4 have been obtained. The model of Section 6 has been worked out with F. Pétrélis and its application to the geodynamo resulted from a collaboration we had with E. Dormy and J.P. Valet. Finally, the simulations presented in Section 7 have been performed by E. Dormy and C. Gissinger.

References

[1] P. Abry, S. Fauve, P. Flandrin, and C. Laroche, Analysis of pressure fluctuations in swirling turbulent flows. J. Physique II **4**, 725–733 (1994).

[2] G. Ahlers & R.P. Behringer, Evolution of turbulence from the Rayleigh–Bénard instability, Phys. Rev. Lett. **40**, 712–716 (1978).

[3] D.W. Allan, *On the behavior of systems of coupled dynamos*. Proc. Camb. Phil. Soc. **58**, 671–693 (1962).

[4] J. Aubert, J. Aurnou & J. Wicht, The magnetic structure of convection-driven numerical dynamos. Geophys. J. Int. **172**, 945–956 (2008).

[5] S. Aumaître, *et al.*, The VKS experiment: Turbulent dynamical dynamos. Phys. Fluids **21**, 035108 (2009).

[6] D. Armbruster, P. Chossat & I. Oprea, *Structurally stable heteroclinic cycles and the dynamo dynamics*, In *Dynamo and Dynamics, a Mathematical Challenge* (eds. Chossat P., Armbruster D. & Oprea I) (2001), pp. 313–322, Nato Science Series II, vol 26, Kluwer Academic Publishers.

[7] V. Arnold, *Geometrical Methods in the Theory of Ordinary Differential Equations*, Springer-Verlag (1982).

[8] M. Berhanu, *et al.*, Magnetic field reversals in an experimental turbulent dynamo. Europhys. Lett. **77**, 59001 (2007).

[9] M. Bourgoin, *et al.*, Magnetohydrodynamics measurements in the von Kármán sodium experiment. Phys. Fluids **14**, 3046–3058 (2002).

[10] M. Bourgoin, P. Odier, J.F. Pinton, and Y. Ricard, An iterative study of time independent induction effects in magnetohydrodynamics. *Phys. Fluids* **16**, 2529–2547 (2004).

[11] B. Brunhes, Recherches sur la direction d'aimantation des roches volcaniques. J. de Phys. Théor. App. **5**, 705–724 (1906).

[12] F.H. Busse, *Mathematical problems of dynamo theory*, In *Applications of bifurcation theory* (1977) pp. 175–202, Academic Press.

[13] F.H. Busse, U. Müller, R. Stieglitz & A. Tilgner, A two-scale homogeneous dynamo, and extended analytical model and an experimental demonstration under development. Magnetohydrodynamics **32**, 235–248 (1996).

[14] F.H. Busse & R. Simitev, Parameter dependences of convection driven dynamos in rotating spherical fluid shells. GAFD **100**, 341–361 (2006).

[15] M. Ghil & S. Childress, Topics in geophysical fluid dynamics: atmospheric dynamics, dynamo theory, and climate dynamics. Appl. Math. Sci. **60** (1987), New York: Springer Verlag.

[16] P. Chossat & D. Armbruster, Dynamics of polar reversals in spherical dynamos. Proc. Roy. Soc. Lond. A **459**, 577–596 (2003).

[17] R.S. Coe, L. Hongre & G.A. Glatzmaier, An examination of simulated geomagnetic reversal from a paleomagnetic perspective. Phil. Transact. Royal Soc. A **358**, 1141–1170 (2000).

[18] A.E. Cook & P.H. Roberts, The Rikitake two-disc dynamo system. Proc. Camb. Phil. Soc. **68**, 547–569 (1970).

[19] E. Dormy, J.-P. Valet & V. Courtillot, Numerical models of the geodynamo and observational constraints. Geochem. Geophys. Geosyst. **1**, 2000GC000062 (2000).

[20] S. Fauve, C. Laroche, and B. Castaing, Pressure fluctuations in swirling turbulent flows. J. Physique II **3**, 271–278 (1993).

[21] S. Fauve, C. Laroche, A. Libchaber & B. Perrin, Chaotic Phases and Magnetic Order in a Convective Fluid. Phys. Rev. Lett. **52**, 1774–1777 (1984).

[22] S. Fauve & D.P. Lathrop, *Laboratory Experiments on Liquid Metal Dynamos and Liquid Metal MHD Turbulence*. In Fluid Dynamics and Dynamos in Astrophysics and Geophysics, (ed. Soward, A. *et al.*, (2003), pp. 393–425.

[23] S. Fauve & F. Pétrélis, *The dynamo effect*. In Peyresq Lectures on Nonlinear Phenomena, vol. II (2003), pp. 1–64 (ed. Sepulchre, J.-A.) Singapore: World Scientific.

[24] S. Fauve & F. Pétrélis, Scaling laws of turbulent dynamos. C. R. Physique **8**, 87–92 (2007).

[25] M.J. Feigenbaum, Quantitative universality for a class of nonlinear transformations. J. Stat. Phys. **19**, 25–52 (1978).

[26] A. Gailitis, O. Lielausis, E. Platacis, S. Dement'ev, A. Cifersons, G. Gerbeth, T. Gundrum, F. Stefani, M. Christen and G. Will, Magnetic field saturation in the Riga dynamo experiment. Phys. Rev. Lett. **86**, 3024–3027 (2001).

[27] A. Gailitis, O. Lielausis, E. Platacis, E. Dement'ev, A. Cifersons, G. Gerbeth, T. Gundrum, F. Stefani, M., Christen, and G. Will, Dynamo experiments at the Riga sodium facility. Magnetohydrodynamics **38**, 5–14 (2002).

[28] A. Giesecke, G. Rüdiger & D. Elstner, Oscillating α^2-dynamos and the reversal phenomenon of the global geodynamo. Astron. Nach. **326**, 693–700 (2005).

[29] A. Giesecke, F. Stefani & G. Gerbeth, Role of Soft-Iron Impellers on the Mode Selection in the von Kármán–Sodium Dynamo Experiment. Phys. Rev. Lett. **104**, 044503 (2010).

[30] C. Gissinger, A. Iskakov, S. Fauve & E. Dormy, Effect of magnetic boundary conditions on the dynamo threshold of von Karman swirling flows. Europhys. Lett. **82**, 29001 (2008).

[31] C. Gissinger, E. Dormy & S. Fauve, Bypassing Cowling's theorem in axisymmetric fluid dynamos. Phys. Rev. Lett. **101**, 144502 (2008).

[32] C.J.P. Gissinger, A numerical model of the VKS experiment. Europhys. Lett. **87**, 39002 (2009).

[33] C. Gissinger, E. Dormy & S. Fauve, Morphology of field reversals in turbulent dynamos. Europhys. Lett. **90**, 49001 (2010).

[34] G.A. Glatzmaier & P.H. Roberts, A three-dimensional self-consistent computer simulation of a geomagnetic field reversal. Nature **3**77, 203–209 (1995).

[35] J.P. Gollub & H.L. Swinney, Onset of Turbulence in a Rotating Fluid. Phys. Rev. Lett. **3**5, 927–930 (1975).

[36] P. Hoyng & J.J. Duistermaat, Geomagnetic reversals and the stochastic exit problem. Europhys. Lett. **68** (2), 177–183 (2004).

[37] D. Hughes & M.R.E. Proctor, A low-order model for the shear instability of convection: chaos and the effect of noise. Nonlinearity **3**,127–153 (1990).

[38] E. Knobloch & A.S. Landsberg, A new model for the solar cycle. Mon. Not. R. Astron. Soc. **278**, 294–302 (1996).

[39] E. Knobloch, S.M. Tobias & N.O. Weiss, Modulation and symmetry changes in stellar dynamos. Mon. Not. R. Astron. Soc. **297**, 1123–1138 (1998).

[40] R. Krishnamurti & L.N. Howard, Large-scale flow generation in turbulent convection. Proc. Natl. Sci. USA **78**,1981–1985 (1981).

[41] C. Kutzner & U.R. Christensen, From stable dipole towards reversing numerical dynamos. Physics of the Earth and Planetary Interior **131**, 29–45 (2002).

[42] R. Laguerre, *et al.*, Impact of Impellers on the Axisymmetric Magnetic Mode in the VKS2 Dynamo Experiment. Phys. Rev. Lett. **101**, 104501 and 219902 (2008).

[43] L.D. Landau, and E.M. Lifshitz, *Fluid Mechanics*. Oxford: Pergamon (1959).

[44] J. Larmor, *How could a rotating body such as the sun become a magnet?*. Rep. 87$^{\text{th}}$ Meeting Brit. Assoc. Adv. Sci. Bornemouth, Sept. 9–13, 1919 pp. 159–160, London:John Murray.

[45] E.H. Levy, Kinematic reversal schemes for the geomagnetic dipole. Astophys. J. **171**, 635–642 (1972).

[46] A. Libchaber, C. Laroche & S. Fauve, Period doubling cascade in mercury, a quantitative measurement. J. Physique Lettres **43**, 211–216 (1982).

[47] B. Liu & J. Zhang, Self-Induced Cyclic Reorganization of Free Bodies through Thermal Convection. Phys. Rev. Lett. **1**00, 244501 (2008).

[48] E. Lorenz, Deterministic non periodic flow. Journal of the Atmospheric Sciences **2**0, 130–141 (1963).

[49] W.V.R. Malkus, Reversing Bullard's dynamo. EOS Tran. Am. Geophys. Union **53**, 617 (1972).

[50] P. Manneville & Y. Pomeau, Intermittency and the Lorenz model. Phys. Lett. **A** 75, 1–2 (1979).

[51] L. Marié, J. Burguete, F. Daviaud, and J. Léorat, Numerical study of homogeneous dynamo based on experimental von Kármán type flows. Eur. Phys. J. B **33**, 469–485 (2003).

[52] J. Maurer & A. Libchaber, Rayleigh–Bénard experiment in liquid helium; frequency locking and the onset of turbulence. J. Physique Lettres **40**, 419–423 (1979).

[53] P.L. McFadden, R.T. Merril & M.W. McElhinny, Dipole/quadrupole family modeling of paleosecular variations. J. Geophys. Research **93**, 11583–11588 (1991).

[54] P.L. McFadden & R.T. Merrill, Fundamental transitions in the deodynamo as suggested by palaeomagnetic data. Physics of the Earth and Planetary Interior **9**1, 253–260 (1995).

[55] I. Melbourne, M.R.E. Proctor & A.M. Rucklidge, *A heteroclinic model of geodynamo reversals and excursions*. In Dynamo and Dynamics, a Mathematical Challenge (eds. Chossat P., Armbruster D. & Oprea I.), pp. 363–370, Nato Science Series II, vol. 26 (2001), Kluwer Academic Publishers.

[56] H.K. Moffatt, *Magnetic Field Generation in Electrically Conducting Fluids*. Cambridge: Cambridge University Press (1978).

[57] R. Monchaux, *et al.*, Generation of a magnetic field by dynamo action in a turbulent flow of liquid sodium. Phys. Rev. Lett. **98**, 044502 (2007).

[58] R. Monchaux, *et al.*, *The von Kármán Sodium experiment: Turbulent dynamical dynamos*. Phys. Fluids **21**, 035108 (2009).

[59] N. Nishikawa & K. Kusano, Simulation study of the symmetry-breaking instability and the dipole field reversal in a rotating spherical shell dynamo. Physics of Plasma **15**, 082903 (2008).

[60] P. Nozières, Reversals of the Earth's magnetic field: an attempt at a relaxation model. Physics of the Earth and Planetary Interior **17**, 55–74 (1978).

[61] D. Sweet, E. Ott, J. Finn, T.M. Antonsen & D.A. Lathrop, Blowout bifurcations and the onset of magnetic activity in turbulent dynamos. Phys. Rev. **E 63**, 066211 (2001).

[62] E.N. Parker, Hydromagnetic dynamo models. Astophys. J. **122**, 293–314 (1955).

[63] E.N. Parker, The occasional reversal of the geomagnetic field. Astophys. J. **158**, 815–827 (1969).

[64] E.N. Parker, *Cosmical magnetic Fields*. Oxford: Clarendon Press (1979).

[65] F. Pétrélis & S. Fauve, Saturation of the magnetic field above the dynamo threshold. Eur. Phys. J. B **22**, 273–276 (2001).

[66] F. Pétrélis, M. Bourgoin, L. Marié, J. Burgete, A. Chiffaudel, F. Daviaud, S. Fauve, P. Odier, and J.F. Pinton, Nonlinear magnetic induction by helical motion in a liquid sodium turbulent flow. Phys. Rev. Lett. **9**0, 174501 (2003).

[67] F. Pétrélis, E. Dormy, J.-P. Valet & S. Fauve, Simple mechanism for the reversals of Earth magnetic field. Phys. Rev. Lett. **1**02, 144503 (2009).

[68] F. Pétrélis & S. Fauve, Chaotic dynamics of the magnetic field generated by dynamo action in a turbulent flow. J. Phys.: Condens. Matter **20**, 494203 (2008).

[69] F. Pétrélis, N. Mordant & S. Fauve, On the magnetic fields generated by experimental dynamos. G. A. F. D. **101**, 289–323 (2007).

[70] Yu.B. Ponomarenko, Theory of the hydromagnetic generator. Appl. Mech. Tech. Phys. **14**, 775–778 (1973).

[71] F. Ravelet, A. Chiffaudel, F. Daviaud, and J. Léorat, Toward an experimental von Kármán dynamo: Numerical studies for an optimized design. Phys. Fluids **17**, 117104 (2005).

[72] F. Ravelet, *et al.*, Chaotic dynamos generated by a turbulent flow of liquid sodium. Phys. Rev. Lett. **101**, 074502 (2008).

[73] T. Rikitake, Oscillations of a system of disc dynamos. Proc. Camb. Phil. Soc. **54**, 89–105 (1958).

[74] G.O. Roberts, Dynamo action of fluid motions with two-dimensional periodicity. Phil. Trans. Roy. Soc. London A **271**, 411–454 (1972).

[75] P.H. Roberts, Kinematic dynamo models. Phil. Trans. Roy. Soc. London A **272**, 663–698 (1972).

[76] P.H. Roberts, *Dynamo theory.* Irreversible phenomena an dynamical systems analysis in geosciences, (eds. Nicolis C. & Nicolis G.), Reidel Publishing Company (1987).

[77] P.H. Roberts, *Fundamentals of dynamo theory.* In Lectures on solar and planetary dynamos, chap. 1, pp. 1–57, eds. M.R.E. Proctor & A.D. Gilbert, Cambridge University Press (1994).

[78] P.H. Roberts & G.A. Galtzmaier, Geodynamo theory and simulations. Rev. Mod. Phys. **72**, 1081–1123 (2000).

[79] K.A. Robbins, A new approach to subcritical instability and turbulent transitions in a simple dynamo. Math. Proc. Camb. Phil. Soc. **82**, 309–325 (1977).

[80] D. Ruelle & F. Takens, On the nature of turbulence. Commun. Math Phys. **20**, 167–192 (1971).

[81] G.R. Sarson, Reversal models from dynamo calculations. Phil. Trans. R. Soc. Lond. A **358**, 921–942 (2000).

[82] G.R. Sarson & C.A. Jones, A convection driven geodynamo reversal model. Physics of the Earth and Planetary Interior **111**, 3–20 (1999).

[83] D. Schmitt, M.A.J.H. Ossendrijver & P. Hoyng, Magnetic field reversals and secular variation in a bistable dynamo model. Physics of the Earth and Planetary Interior **125**, 119–124 (2001).

[84] J. Sommeria, Experimental study of the two-dimensional inverse energy cascade in a square box. J. Fluid Mech. **170**, 139–168 (1986).

[85] F. Stefani & G. Gerbeth, Asymmetric polarity reversals, bimodal field distribution and coherence resonance in a spherically symmetric mean-field dynamo model. Phys. Rev. Lett. **94**, 184506 (2005).

[86] F. Stefani, M. Xu, G. Gerbeth, F. Ravelet, A. Chiffaudel, F. Daviaud, and J. Léorat, Ambivalent effects of added layers on steady kinematic dynamos in cylindrical geometry: application to the VKS experiment. Eur. J. Mech. B **25**, 894 (2006).

[87] F. Stefani, M. Xu, L. Sorriso-Valvo, G. Gerbeth & U. Günther, Oscillation or rotation: a comparison of two simple reversal models. Geophysical and Astrophysical Fluid Dynamics **101**, 227–248 (2007).

[88] R. Stieglitz & U. Müller, Experimental demonstration of a homogeneous two-scale dynamo. Phys. Fluids **13**, 561–564 (2001).

[89] R. Stieglitz & U. Müller, Experimental demonstration of a homogeneous two-scale dynamo. Magnetohydrodynamics **38**, 27–34 (2002).

[90] E. Stone & P. Holmes, Random Perturbations of Heteroclinic Attractors. SIAM J. Appl. Math. **5**0, 726–743 (1990).

[91] S.M. Tobias, N.O. Weiss & V. Kirk, Chaotically modulated stellar dynamos. Mon. Not. R. Astron. Soc. **273**, 1150–1166 (1995).

[92] C. Tresser & P. Coullet, Itèrations d'endomorphismes et groupe de renormalisation. C. R. Acad. Sci. Paris **A 287**, 577–580 (1978).

[93] J.-P. Valet, L. Meynadier & Y. Guyodo, Geomagnetic field strength and reversal rate over the past 2 Million years. Nature **435**, 802–805 (2005).

[94] G.K. Vallis, El Nino: A Chaotic Dynamical System? Science **232**, 243–245 (1986).

[95] G. Verhille, *et al.*, Induction in a von Kármán flow driven by ferromagnetic impellers. New Journal of Physics **12**, 033006 (2010).

[96] J. Wicht & P. Olson, A detailed study of the polarity reversal mechanism in a numerical dynamo model. Geochemistry, Geophysics, Geosystems **5**, Q03GH10 (2004).

[97] A.L. Wilmot-Smith, P.C.H. Martens, D. Nandy, E.R. Priest & S.M. Tobias, Low order stellar dynamo models. Mon. Not. R. Astron. Soc. **363**, 1167–1172 (2005).

[98] P.J. Zandbergen & D. Dijkstra, von Kármán swirling flows. Annu. Rev. Fluid Mech. **19**, 465–491 (1987).

[99] Ya.B. Zeldovich, A.A. Ruzmaikin & D.D. Sokoloff, *Magnetic fields in astrophysics*. New York: Gordon and Breach (1983).

Stéphan Fauve
École Normale Supérieure
24, rue Lhomond
F-75005 Paris, France
e-mail: fauve@lps.ens.fr

http://www.springer.com/978-3-0348-0696-1

Chaos
Poincaré Seminar 2010
Duplantier, B.; Nonnenmacher, S.; Rivasseau, V. (Eds.)
2013, XII, 270 p. 100 illus., 61 illus. in color., Hardcover
ISBN: 978-3-0348-0696-1
A product of Birkhäuser Basel